Communications Research Centre

A MICROWAVE FET OSCILLATOR DESIGN APPROACH AND ITS APPLICATION IN AN INJECTION-LOCKED OSCILLATOR

by

P. MORRISON AND R. DOUVILLE

CRC REPORT NO. 1347

Department of Communications
Ministère des Communications

OTTAWA, JANUARY 1982

COMMUNICATIONS RESEARCH CENTRE

DEPARTMENT OF COMMUNICATIONS
CANADA

A MICROWAVE FET OSCILLATOR DESIGN APPROACH AND ITS APPLICATION IN AN INJECTION-LOCKED OSCILLATOR

by

P. Morrison and R. Douville

(Space Technology and Applications Branch)

CRC REPORT NO. 1347

January 1982

OTTAWA

TABLE OF CONTENTS

ABSTRACT 1

1. INTRODUCTION 1

2. DESIGN APPROACH 2

2.1 Introduction 2

2.2 Circuit Configuration and Model 2

2.3 Output Admittance vs Transmission Line Lengths 7

2.4 Large Signal Effects 7

2.5 Coupling 10

2.6 Spurious Suppression 10

2.7 Injection-Locked Bandwidth – Q_{ext} Effects 11

2.8 Output Match 13

2.9 Comparison with Another Design Approach 13

3. OSCILLATOR DESIGN 14

4. OSCILLATOR PERFORMANCE 15

4.1 Y_{out} versus Frequency (Small Signal) 15

4.2 Free-Running Performance 15

4.3 Injection-Locked Performance 16

4.3.1 Gain versus Bandwidth 16

4.3.2 FM Noise Performance 16

4.3.3 Transient Response 17

5. CONCLUSIONS AND RECOMMENDATIONS 17

6. REFERENCES 18

A MICROWAVE FET OSCILLATOR DESIGN APPROACH AND ITS APPLICATION IN AN INJECTION-LOCKED OSCILLATOR

by

P. Morrison and R. Douville

ABSTRACT

A low power 14 GHz MIC GaAs FET oscillator has been designed. The analytical model of the oscillator and design approach used are discussed in detail.

A shunt feedback oscillator configuration was employed. Approximations were made to account for FET large signal effects in the design for maximum oscillator output power. An expression relating oscillator output power to feedback loop loss is presented. The requirement for filtering in the feedback loop is discussed.

Experimental results are compared with theory and found to be in good agreement. Output power was 10 dBm at 14.0 GHz. The injection-locked characteristics of the oscillator were experimentally investigated. It was found that for a 15 dB injection gain, the locking bandwidth was 69 MHz. The FM noise properties and transient performance of the injection-locked oscillator are presented.

1. INTRODUCTION

This technical report describes the development of a 14 GHz low-power microwave-integrated-circuit gallium arsenide field-effect transistor (MIC GaAs FET) oscillator. The basic objectives of this study were two-fold - first, to develop an MIC oscillator design procedure and secondly to evaluate

the oscillator's injection-locked performance for possible use as a gain stage in a 2-way telephony transmitter.

The design procedure development had the following goals. Large signal effects were to be accounted for in order that a design with maximum output power could be attempted. The design procedure was intended to be applicable to future oscillator development and in particular to high power units. Low FM noise was not a particular requirement.

The injection-locked oscillator was intended to replace a two-stage amplifier for use in a 2-way telephony terminal. As such, it was to provide an injection gain of at least 15 dB across the 500 MHz Ku satellite communications band (14.000 to 14.500 GHz) or, as a minimum, across the 54 MHz bandwidth of a single transponder. The output power across the locking bandwidth was to be about 10 dBm. Low FM noise in the free-running mode was not a requirement since, for the narrow data bandwidths under consideration here, stability could readily be provided by the injection source.

2. DESIGN APPROACH

2.1 INTRODUCTION

The oscillator design technique used here is a combination of the one-port and the "classical" feedback approaches. The oscillator, viewed as a one port, and the load were designed such that the sum of their admittances was zero at the desired oscillation frequency. Also, the ratio of the power fed back to the input of the FET to that dissipated in the load (i.e. the coupling ratio) was selected with a view to maximizing the power delivered to the load. In the structure used, the functions of the various oscillator components are intermingled. The amplitude-limiting function, essential for the determination of the output power, was provided by the FET's signal level dependent non-linearity. In the following sections, the oscillator design parameters are presented. Also, it is shown how this design technique can be compared to another approach.

2.2 CIRCUIT CONFIGURATION AND MODEL

A shunt feedback oscillator configuration was used and is shown in functional form in Figure 1. This permits the FET's source to be grounded in order that this approach be directly applicable to high power designs where heat dissipation is a prime concern. This feedback loop approach is conceptually easy to understand and facilitates power coupling (output-to-input) calculations (see Section 2.5). Note that input and output matching networks (stubs, transformers, etc.) for the FET are not used within the loop. This very simple configuration was selected to minimize the oscillator's Q (see Section 2.7). The microstrip realizations of the coupler and feedback loop are as follows:

i) *Coupler*: A symmetric 50 ohm "T" junction was used to couple power from the device's output back to its input. A sketch

of the "T" junction and the equivalent circuit used for it here are given in Figures 2a and 2b. A computer program* based on Hammerstad's[1] semi-empirical expressions was used to calculate values for the parameters in the equivalent circuit. For use as a coupler or divider, the "T" junction is very simple, compact, wideband, relatively lossless and the coupling ratio can easily be varied over a wide range simply by changing the terminating impedances.

ii) *Feedback Loop*: The feedback loop component used was a 50 ohm transmission line whose length was adjusted to satisfy the various design goals. As will be described in Section 2.6, a filter was later incorporated into the feedback loop but for purposes of analysis and design it is sufficient to model the loop as a transmission line.

The one-port model of the oscillator is then as given in Figure 3a. The "T" junction reference plane shifts are included in the line lengths given in the figure and were accounted for in the circuit realization. The design variables used were the feedback loop length, θ_1, and the output line length, θ_{op}. If it had been necessary, another degree of freedom could have been obtained by varying the transmission line characteristic impedance. The parameters of interest ($\overline{y_c}$, $\overline{y_{out}}$, $[\overline{y}]$, $[\overline{s}]$, $[\overline{y'}]$, $[\overline{y''}]$, $[\overline{y_f}]$) mentioned in the discussion which follows are identified in Figures 3b to 3e. The bars above the admittance parameters indicate they are normalized with respect to the transmission line characteristic admittance. The [s] and $[\overline{y}]$ matrices refer to the FET itself. The $[\overline{y'}]$ matrix refers to the series combination of the FET plus the output transmission line, θ_{op}. The $[\overline{y''}]$ matrix refers to the series combination of the "T" junction shunt susceptance ($\overline{b_{jn}}$), the "T" junction transformer, the feedback line (θ_1), the FET and the output line (θ_{op}). The $[\overline{y_f}]$ matrix describes the feedback loop. The admittance, $\overline{y_{out}}$, is that which occurs when the loop is closed. $\overline{y_c}$ is the feedback admittance seen at the centre of the "T" junction, looking back towards the gate, in the closed loop configuration. Because the device is not unilateral, $\overline{y_c}$ is affected by both the load, y_L and θ_{op}.

The general equations for these parameters are:

$$[\overline{y}] = \begin{bmatrix} \overline{y}_{11} & \overline{y}_{12} \\ \overline{y}_{21} & \overline{y}_{22} \end{bmatrix} \qquad (1)$$

---

* TJ - developed by M. Cuhaci

$$\text{where: } \overline{y}_{11} = \frac{(1-S_{11})\ (1+S_{22}) + S_{12}\ S_{21}}{D}$$

$$\overline{y}_{12} = \frac{-\ 2\ S_{12}}{D}$$

$$\overline{y}_{21} = \frac{-\ 2\ S_{21}}{D}$$

$$\overline{y}_{22} = \frac{(1+S_{11})\ (1-S_{22}) + S_{12}\ S_{21}}{D}$$

$$D = (1 + S_{11})\ (1 + S_{22}) - S_{12}\ S_{21}$$

$$[\overline{y}] = \begin{bmatrix} \overline{y}_{11}' & \overline{y}_{12}' \\ \overline{y}_{21}' & \overline{y}_{22}' \end{bmatrix} \qquad (2)$$

$$\text{where: } \overline{y}_{11}' = \frac{(1-S_{11}')\ (1+S_{22}') + S_{12}'\ S_{21}'}{D'}$$

$$\overline{y}_{12}' = \frac{-\ 2\ S_{12}'}{D'}$$

$$\overline{y}_{21}' = \frac{-2\ S_{21}'}{D'}$$

$$\overline{y}_{22}' = \frac{(1+S_{11}')\ (1-S_{22}') + S_{12}'\ S_{21}'}{D'}$$

$$D' = (1+S_{11}')\ (1+S_{22}') - S_{12}'\ S_{21}'$$

and

$$S_{11}' = |S_{11}| \angle \theta_{11}$$

$$S_{12}' = |S_{12}| e^{-\alpha\theta_{op}} \angle \theta_{12} - \theta_{op}$$

$$S_{21}' = |S_{21}| e^{-\alpha\theta_{op}} \angle \theta_{21} - \theta_{op}$$

$$S_{22}' = |S_{22}| e^{-2\alpha\theta_{op}} \angle \theta_{22} - 2\theta_{op}$$

γ = transmission line propagation constant

$= \beta - j\alpha$

$$[\overline{y}''] = \begin{bmatrix} \overline{y}_{11}'' & \overline{y}_{12}'' \\ \overline{y}_{21}'' & \overline{y}_{22}'' \end{bmatrix} \qquad (3)$$

where: $\overline{y_{11}}'' = \overline{jb_{jn}} - j \left[\frac{n_2}{n_1}\right]^2 \cot \gamma l_1 + \frac{\left[\frac{n_2}{n_1}\right]^2 \csc^2 \gamma l_1}{\overline{y}_{11}' - j \cot \gamma l_1}$

$$\overline{y}_{12}'' = \frac{\overline{y}_{12}' \left(-j\left[\frac{n_2}{n_1}\right] \csc \gamma l_1\right)}{\overline{y}_{11}' - j \cot \gamma l_1}$$

$$\overline{y}_{21}'' = \frac{\overline{y}_{21}' \left(-j \left[\frac{n_2}{n_1}\right] \csc \gamma l\right)}{\overline{y}_{11}' - j \cot \gamma l_1}$$

$$\overline{y}_{22}'' = \overline{y}_{22}' - \frac{\overline{y}_{12}' \overline{y}_{21}'}{\overline{y}_{22}' - j \cot \gamma l_1}$$

$$\overline{y}_{out} = \overline{y}_{11}'' + \overline{y}_{12}'' + \overline{y}_{21}'' + \overline{y}_{22}'' \tag{4}$$

$$\overline{y}_c = \frac{-B_c \pm \sqrt{B_c^2 - 4\,A_c\,C_c}}{2A_c} \tag{5}$$

where: $A_c = C$

$B_c = CE - (AC+B) + D$

$C_c = -(E(AC+B)+AD)$

and: $A = \overline{jb_{jn}} - j\left(\frac{n_2}{n_1}\right)^2 \cot \gamma l_1$

$B = \left(\frac{n_2}{n_1}\right)^2 \csc^2 \gamma l_1$

$C = \overline{y}_{11}' - j \cot \gamma l_1$

$D = -\overline{y}_{12}'\overline{y}_{21}'$

$E = \overline{y}_{22}' + \overline{y}_L$

$$[y_f] = \begin{bmatrix} \overline{y}_{f11} & \overline{y}_{f12} \\ \overline{y}_{f21} & \overline{y}_{f22} \end{bmatrix} \tag{6}$$

where: $\overline{y}_{f11} = -j \cot \gamma l_1$

$\overline{y}_{f12} = j\left(\frac{n_2}{n_1}\right) \csc \gamma l_1$

$$\overline{y}_{f21} = j\left(\frac{n_2}{n_1}\right)\csc \gamma l_1$$

$$\overline{y}_{f22} = -j\left(\frac{n_2}{n_1}\right)^2 \cot \gamma l_1 + j\,\overline{b}_{jn}$$

2.3 OUTPUT ADMITTANCE VS TRANSMISSION LINE LENGTHS

Using equation (4), $\overline{y_{out}}$ was calculated at 14.25 GHz and is plotted in Figure 4 versus θ_1 with θ_{op} as a parameter. In this figure, each curve has a constant value of θ_{op} and the end point values of θ_1 are indicated. The increment of θ_1 is 10°. Measured small signal S-parameters of the NEC38883 FET at 14.25 GHz were utilized in the above calculations and are given below:

$S_{11} = .77\angle 146°$
$S_{12} = .07\angle 14°$
$S_{21} = 1.06\angle -50°$
$S_{22} = .68\angle -180°$

$V_g = -1.67$ volts
$V_d = +3.0$ volts
$I_d = 20.0$ mA
$f = 14.25$ GHz

} Operating Conditions

The FET bias levels shown are the same as those used in a two-way telephony two-stage preamplifier. From Figure 4, it is evident that if only the one-port resonance condition mentioned in Section 2.1 is considered (i.e. $\overline{Y_L} + \overline{Y_{out}} = 0$), then a wide range of (θ_1, θ_{op}) combinations are possible at which oscillations may occur.

2.4 LARGE SIGNAL EFFECTS

One of the design goals was that the oscillator operate at maximum output power. Large signal effects and saturation characteristics must therefore be taken into account. The approach taken here is based upon observations by Maeda et al[1] and Johnson[3] and makes the assumptions that the only significant change in the device characteristics versus signal level is in $|S_{21}|$, and all others remain constant at their small signal values. It was felt that these assumptions would not result in significant degradation of the oscillator's performance but this was to be verified. In Figure 5, $\overline{y_{out}}$ is plotted on the negative Smith chart with $|S_{21}|$ as a parameter for $\theta_{op} = 55°$. From this figure it is obvious that, as $|S_{21}|$ varies from small to large signal values, the phase of S_{21} and, therefore, the oscillation frequency do not change radically.

Johnson[3] outlined an approach for determining the optimum large signal operating point for maximum efficient gain, G_{ME}, based upon the amplifier's P_{out} vs P_{in} curve. G_{ME} is the gain at which the two-port added power is maximum for a given value of input power, and is therefore, particularly suited to oscillator and large signal amplifier design. Also, G_{ME} is a

useful figure of merit since it is well behaved even in the frequency regions where the device is potentially unstable. The maximum efficient gain is given by:

$$G_{ME} = \frac{\left|\frac{S_{21}}{S_{12}}\right|^2 - 1}{2\left(K\left|\frac{S_{21}}{S_{12}}\right| - 1\right)} \tag{7}$$

where: K = Rollett stability factor

$$= \frac{1 + |S_{11}S_{22}-S_{21}S_{12}|^2 - |S_{11}|^2 - |S_{22}|^2}{2|S_{12}S_{21}|}$$

Johnson's analysis has been extended here to include the effects of any feedback loop losses (or gains) as follows. The model for the feedback oscillator is given in Figure 6. The P_{out} vs P_{in} curve (Figure 7) is described by the following equation which has been found to be very accurate in practice (3).

$$P_o = P_{sat}\left(1 - e^{\frac{-G_o P_i}{P_{sat}}}\right) \tag{8}$$

Also:

$$P_i = L\,P_c \tag{9}$$

$$P_o = P_{sat}\left(1 - e^{\frac{-G_o L P_c}{P_{sat}}}\right) \tag{10}$$

$$P_{osc} = P_{sat}\left(1 - e^{\frac{-G_o L P_c}{P_{sat}}}\right) - P_c \tag{11}$$

where L = feedback loop loss

P_i = input power

P_o = output power

P_{sat} = saturated output power

G_o = small signal gain (G_{ME} calculated with small signal S parameters)

At the point of maximum oscillator output power,

$$P_{i/opt} = \frac{P_{sat}}{G_o} \ln LG_o \tag{12}$$

$$P_{o/opt} = P_{sat} \left(1 - \frac{1}{LG_o}\right) \tag{13}$$

$$P_{osc/opt} = P_{sat} \left(1 - \frac{1}{LG_o} - \frac{\ln LG_o}{LG_o}\right) \tag{14}$$

and

$$G_{ME/opt} = \frac{G_o - 1/L}{\ln LG_o} \tag{15}$$

$P_{osc/opt}$, normalized with respect to P_{sat}, is plotted in Figure 8 versus L, the loop loss, for G_o = 10.3 dB. From this it can be seen that, even for zero loop loss, the maximum oscillator output power is 1.7 dB less than the device's saturated output power.

$|S_{21}|_{opt}$ is the value of $|S_{21}|$ which corresponds to maximum oscillator output power and is given by:

$$|S_{21}|_{opt} = \frac{-B \mp \sqrt{B^2 - 4AC}}{2A} \tag{16}$$

where: $A = |S_{12}|^2 G_{ME/opt} - 1$

$$B = -2G_{ME/opt}|S_{12}||S_{21}||S_{22}|\cos(\theta_{11} + \theta_{22} - \theta_{12} - \theta_{21})$$

$$C = G_{ME/opt}(1+|S_{11}|^2|S_{22}|^2-2|S_{12}|^2-|S_{11}|^2-|S_{22}|^2)+|S_{12}|^2$$

The above relationship is based on the assumption that all S parameters other than $|S_{21}|$ are constant at their small signal values.

R_{opt} is the ratio of coupled power P_c, to power dissipated in the load, P_L, corresponding to $|S_{21}|_{opt}$ and is given by:

$$R_{opt} = \frac{\ln LG_o}{LG_o - 1 - \ln (LG_o)} \tag{17}$$

Plots of $|S_{21}|_{opt}$ and R_{opt} versus L (feedback loop loss) are given in Figure 9.

2.5 COUPLING

R, the ratio of the power coupled back to the FET's input to the power absorbed in the load is given by:

$$R = \frac{P_c}{P_L} = \frac{\overline{g}_c}{\overline{g}_L} = \frac{Re(\overline{y}_c)}{Re(\overline{y}_L)} \tag{18}$$

At resonance $\overline{y}_L = -\overline{y}_{out}$ so R becomes:

$$R = \frac{Re\ (\overline{y}_c)}{-Re\ (\overline{y}_{11}'' + \overline{y}_{12}'' + \overline{y}_{21}'' + \overline{y}_{22}'')}$$

$$= \frac{\overline{g}_c}{-(\overline{g}_{11}'' + \overline{g}_{12}'' + \overline{g}_{21}'' + \overline{g}_{22}'')} \tag{19}$$

This is plotted in Figure 10 versus θ_1 with θ_{op} as a parameter for $|S_{21}| = .81$. The value of $|S_{21}|$ used here is calculated in Section 3.0. Since the coupling ratio is a function of the feedback loop length, these two parameters cannot be adjusted independently.

2.6 SPURIOUS SUPPRESSION

If a simple transmission line is used for the feedback loop, there is a very good chance that spurious oscillations will occur. This is a particular problem at subharmonic frequencies where the FET's gain is higher. In order to check for spurious oscillations, the model (Figure 3a) must be characterized across the frequency range of concern. For this reason, the NEC 38883 FET's small signal S-parameters were measured on the network analyzer over the range 1 GHz to 18 GHz. A small signal spurious check is sufficient since at large signal levels, gain is reduced and hence tendencies towards spurious oscillations are reduced also. Figure 11 shows the small signal output admittance, $\overline{y_{out}}$ for $\theta_1 = 280°$ and $\theta_{op} = 55°$ across the 1-18 GHz band. This figure illustrates the possibility for operation at a number of subharmonic frequencies as evidenced by the bands of negative resistance between 1.8 and 5.0 GHz, 8.1 and 8.5 GHz and 11.3 and 11.9 GHz.

Filtering is therefore required in the oscillator circuit to shape the loop gain so that the output conductance, $\overline{Y_{out}}$ is negative only in the region of the desired frequency of oscillation. A single resonator coupled-line band pass filter (BPF) was selected since it was found to provide sufficient off-resonance loop gain reduction, and also because it provides dc isolation, thereby eliminating the requirement for a dc blocking capacitor in the feedback loop. The BPF was designed using 50 ohm terminations. When inserted into the feedback loop, the BPF's terminations obviously are dependent upon the device characteristics and the rest of the circuit. At the filter's centre frequency, the transmission line equivalent circuit is valid (180° long for the single resonator BPF); however the out-of-band response can vary widely depending on the terminations. Figures 12 and 13 present the swept frequency (10-16 GHz) output admittance of the oscillator for two different locations of the BPF in the loop*. The oscillator's output admittance with a simple transmission line feedback circuit (i.e. BPF not used) is included in each figure. Near resonance (14.25 GHz where $Z_{out} \simeq 3 + j0\Omega$) the responses are the same but the off-resonance performance is very different. Figure 13 indicates a spurious response at about 10.6 GHz is highly likely. Therefore, in the design it was necessary to step the BPF along the loop until a spurious free response was indicated (e.g. Figure 12).

2.7 INJECTION-LOCKED BANDWIDTH - Q_{ext} EFFECTS

A prime consideration in the oscillator design was its injection-locked bandwidth. Adler's[5] equation relating locking bandwidth (BW_L), power gain (G_p), operating frequency (f_o) and external Q_{ext} is given by**:

$$BW_L = \frac{2f_o}{Q_{ext}} \sqrt{\frac{1}{G_p}} \qquad (20)$$

Therefore, at 14.25 GHz and 15 dB gain the locking bandwidth is:

$$BW_{L/dbMHz} = 73.9 - Q_{ext/dB} \qquad (21)$$

---

* *Note: When the single resonator BPF was inserted into the feedback loop, the length of transmission line in the loop was shortened by 180°.*

** *The use of this equation presupposes approximately a 90° intersection of the device line and impedance locus (5).*

$$\text{where:} \quad BW_{L/dbMHz} = 20\log\left[\frac{BW_L\ (Hz)}{10^6}\right]$$

$$Q_{ext/db} = 20\log Q_{ext}$$

Locking bandwidths of 500 and 54 MHz thus require a Q_{ext} less than about 10 and 92, respectively.

To determine the effects of circuit parameter variations on Q_{ext} and therefore on BW_L, the oscillator when viewed as a one-port was modelled as a parallel resonant circuit (see Figure 14). This is a fairly accurate representation for the case of $\overline{b_{out}} \simeq 0$ at resonance - and is sufficient for Q_{ext} calculations. Close to resonance $\overline{y_{out}}(f)$ can be approximated by:

$$\overline{y_{out}}(f) = \overline{g_{out}}(f) + j\,\overline{b}_{out}(f) \tag{22}$$

$$\text{where:} \quad \overline{g}_{out}(f) \simeq \overline{g}_{out}(f_o)$$

$$b_{out}(f) \simeq \frac{50}{wL}\left[\left[\frac{f}{f_o}\right]^2 - 1\right]$$

$$\text{Now:} \quad Q_{ext} = \frac{1}{w_o L g_L} \simeq \frac{1}{w_o L(-g_{out}(f_o))} \tag{23}$$

$$\text{Therefore:} \quad Q_{ext} \simeq \left[\frac{\frac{f}{f_o}}{\left[\frac{f}{f_o}\right]^2 - 1}\right]\left[\frac{\overline{b_{out}}\ (f)}{(-\overline{g_{out}}\ (f_o)}\right] \tag{24}$$

The above expression was used to determine the effect on Q_{ext} of such parameters as BPF type, signal level and feedback loop length. The most significant observation was that the external Q is strongly dependent on loop length and FET gain, $|S_{21}|$. This is illustrated in Figure 15 for a simple transmission line feedback loop for both small ($|S_{21}| = 1.06$) and large ($|S_{21}| = .81$) signal cases. The graph's abscissa, n, the number of wavelengths at f_o, is related to θ_1 by:

$$\theta_{loop} = \theta_1 + n*360° \tag{25}$$

where: $n = 0,1,2,3,\ldots$

i.e. the feedback loop length is equal to θ_1 plus an integral number, n, of wavelengths at f_o.

This increase of Q with n is as one would expect. If the feedback loop's electrical length is assumed proportional to frequency, then the difference in its electrical length at f_o and f is given by:

$$\Delta\theta = [\theta_{1o} + n * 360\ ]\ [1 - \frac{f}{f_o}] \qquad (26)$$

where θ_{1o} is the line's electrical length at f_o with n=0.

Therefore for a given f_o, f and θ_{1o}, as n increases the phase shift difference increases as well, thus leading to an increase in circuit Q.

Q_{ext} calculations for a single resonator BPF showed a similar trend to that of Figure 15 and predicted a large signal locking bandwidth of approximately 73 MHz for n=1. (θ_{op} = 55°, θ_1 = 280°).

To determine a lower bound on Q_{ext} as a function of the loop's structure, COMPACT was used to embed the FET in a circuit using lumped feedback elements*. The calculated Q_{ext} (large signal) was found to be about 26. To achieve lower external Q values with this same FET would require use of an unpackaged device and lumped/distributed embedding.

2.8 OUTPUT MATCH

The required oscillator load was simply implemented by a single stub 50 ohm to $-y_{out}(f_o)$ match. Use of the stub facilitated adjustment of the load for peaking the output power and frequency. The "T" junction model was used in the stub design.

2.9 COMPARISON WITH ANOTHER DESIGN APPROACH

Vehovec, Houselander, and Spence[7] discussed a two-port embedding technique for maximizing oscillator output power for a known set of device Y parameters. This work was extended by Kotzebue and Parish[8] who derived a set of closed-form solutions for the embedding elements of three series and three shunt oscillators. Johnson[2] subsequently suggested an oscillator design based on the above and the large signal approximation discussed in Section 2.4.

The derivation given by Vehovec et al of the required lumped embedding elements (3 reactances and one load resistance) makes use of an optimum device input-output voltage ratio, A_{opt}, which is calculated from the device y parameters.

---

* *The output transmission line (θ_{op} = 55°) was retained.*

$$A_{/opt} = -\frac{(\bar{y}_{21}+\bar{y}_{12}^{*})}{2\bar{g}_{22}}$$

$$= -\frac{(\bar{g}_{21}+\bar{g}_{12})}{2\bar{g}_{22}} - j\frac{(\bar{b}_{21}-\bar{b}_{12})}{2\bar{g}_{22}} \qquad (27)$$

$$= A_R + jA_I$$

The very simple distributed configuration selected for the oscillator in this study does not readily permit the independent variation/realization of three reactances and a load conductance. However, it is possible to calculate an input-output voltage ratio, A, for this configuration and compare it to A_{opt}. It is convenient here to replace $[\bar{y}]$ elements by $[\bar{y}']$ elements in the A_{opt} equation above. Referring to Figure 16 it is readily shown that A is given by:

$$A = \frac{-(\bar{y}_{f11}+\bar{y}_{f21}) - (\bar{y}_{11}'+\bar{y}_{21}')}{(\bar{y}_{f22}+\bar{y}_{f12})+(\bar{y}_{22}'+\bar{y}_{12}')+\bar{y}_L} \qquad (28)$$

At resonance, $\overline{y_L} = \overline{-y_{out}}$. Therefore, for a particular θ_{op} any y parameter set, A can be plotted versus θ_1, along with A_{opt}, on an (A_R, A_I) coordinate system. Circles of constant output power can be drawn on the (A_R, A_I) system. Figure 17 illustrates this for $\theta_{op} = 55°$ and $|S_{21}| = .81$. Note, in this figure,

$$0 \leq r \leq 1$$

$$P = r * P_{max}$$

where P_{max} occurs at A_{opt}

3. OSCILLATOR DESIGN

The oscillator design followed the approach outlined in the previous Section. Many of the sample charts, graphs, etc., given in that Section were used directly. The circuit was fabricated on a .025" thick, 1" x 1" alumina substrate. The design steps were as follows:

a) The BPF mid-band loss was about 1 to 1.5 dB so the total loop loss was estimated to be approximately 2 dB. The optimum values of $|S_{21}|$ and R were then calculated to be 0.81 and 0.5 respectively.

b) The coupling curves were used to select θ_1 and θ_{op} (280° and 55°, respectively). In this particular case, these line lengths were also selected such that $\overline{b_{out}} \simeq 0$ at the resonant frequency to permit the Q_{ext} equivalent circuit of Section 2.7 to be used directly although this is not necessary in general.

c) The circuit A was compared to A_{opt} and found to be in close agreement ($r \simeq .75$).

d) The BPF was inserted in the feedback loop and its position analytically optimized w.r.t. spurious.

e) The minimum number of excess wavelengths, n, in the feedback loop was found to be 1, as dictated by the physical size of the FET plus the length of the wrap-around shorting tab within the feedback loop (refer to Figure 18). The FET was mounted in a 0.100" diameter hole drilled in the aluminum substrate thus permitting the entire oscillator circuit to be fabricated on a single 1" x 1" substrate. The source tabs could not be much shorter than about 0.040" for ease of soldering. The use of these wrap-around tabs created a narrow-band instability (i.e. $|S_{12}|$ increase), although this did not occur close enough to f_o to cause any spurious problems.

f) The drain stub was designed to match 50 ohms to $\overline{-y_{out}}(f_o)$.

Circuits were fabricated both with and without the drain match stub (Figures 18 and 19). The circuit without the drain stub allowed an output admittance measurement to be made to confirm small signal $\overline{y_{out}}(f)$ and spurious response calculations.

Butterfly networks were used for the gate and drain bias. The output dc block was a 30 pf MIS capacitor.

4. OSCILLATOR PERFORMANCE

4.1 $\overline{Y_{out}}$ VERSUS FREQUENCY (Small Signal)

The small signal swept frequency output admittance of the oscillator, less drain stub, (Figure 19) was measured and the results are compared with calculations in Figure 20. The agreement is seen to be quite good.

4.2 Free-Running Performance

The complete oscillator operated at 14.00 GHz and produced 10 dBm for V_D = 3.0 volts, I_D = 20 mA and V_G = -1.67 volts. In order to peak the output power, some adjustment of the output match was required by means of a chip on the drain stub. Following the discussions of Sections 2.5 and 3.0, the expected output power was approximately 11 dBm*. The measured power is therefore close to that expected. The frequency is about 1.8% lower than the

---

* *Measurements by B. Clarke indicated* P_{sat} = 13.5-14.0 dBm at 14.25 GHz.

design frequency. This offset (≈150-250 MHz) was quite consistent from design-to-design and is attributed to inaccuracies in the measured S parameters, in the large signal approximation, or in the microstrip equivalent circuit. The feedback loop can be shortened by about 8° to 10° to bring the oscillator on frequency while maintaining the peak output power.

4.3 INJECTION-LOCKED PERFORMANCE

4.3.1 Gain versus Bandwidth

The measured injection-locked gain and locking bandwidth are given in Figure 21. At a gain of 15 dB ± .4 dB the locking bandwidth is about 69 MHz. This corresponds to Q_{ext} = 71. The Q_{ext} curve in Figure 21 was calculated from equation 20.

4.3.2 FM Noise Performance

The set-up used for measurement of FM noise is given in Figure 22. It was not possible to measure the free-running oscillator FM noise $F_o(f)$, due to excessive jitter. However, the FM noise was measured at f_o, f_o-30 MHz and f_o + 30 MHz for both injection signal, $F_i(f)$, and the output, or locked, signal, F(f). The output noise spectrum at f_o is given in Figures 23 and 24. No appreciable differences were observed in F(f) at the above frequencies or between F(f) and $F_i(f)$. This suppression of the free-running oscillator's noise is in agreement with the following relation(9):

$$F(f) - F_i(f)_{dB} = 20\log\left[\frac{1 + \alpha * 10^{\frac{(F_o(f)-F_i(f))}{20}}}{1+\alpha}\right] \qquad (29)$$

where $$\alpha = \frac{\left(\frac{f}{B}\right)^2}{1 - \left(\frac{\Delta f}{B}\right)^2}$$

B = 1/2 locking bandwidth

f_i = injection centre frequency

f_o = free-running frequency

f = offset frequency (modulation) w.r.t. f_i

$\Delta f = f_i - f_o$

For the present telephony application, the FM noise suppression would be at a minimum for:

$$\frac{f}{B} \simeq \frac{30\ KHz}{30\ MHz} = .001$$

and $$\frac{\Delta f}{B} = .99$$

From the above, it can be seen that to increase F(f) by $\geq$.1 dB over $F_i(f)$ requires $F_o(f) - F_i(f) \geq 47$ dB. That is, for the relatively narrow modulation bandwidths used here, the injection-locking process provides a great amount of suppression of the free-running oscillator's noise.

The test oscillator (HP626A & MOS-5) was not sufficiently FM noise-free to measure any degradation due to $F_o(f)$. However, since it was only marginally poorer than that of another source whose performance as an L.O. was found to be subjectively acceptable for 2 way telephony, the test was considered to be valid.

4.3.3 Transient Response

For use in a 2 way telephony transmitter, it is necessary that the ILO be switchable (ON/OFF) in the presence of an input signal. During the ON/OFF switching periods, it is important that no spurious are produced in adjacent channels. For this particular ILO, the switching was performed by applying a -1.67(ON)/-3.00(OFF) volt square wave to the gate of the FET. The set-up of Figure 25 was used to examine the ILO transient response. There was a 20 dB difference between the ILO's ON and OFF output power. No spurious signals were observed.

The transient response of an ILO which is switched ON/OFF in the presence of an input locking signal is markedly different than that of an ILO which is left on but the input locking signal is switched ON/OFF as would be the case in conventional voice-activated FM telephony. In the latter case, considerable spurious can occur - this effect is well-documented in the literature[5,10] and was readily observed with the set-up of Figure 25.

5. CONCLUSIONS AND RECOMMENDATIONS

A design procedure has been described for a low-power 14 GHz GaAs FET MIC oscillator. An analytical model of the shunt feedback oscillator is derived and equations presented for output admittance and feedback coupling. An approximation is made for large signal effects in order to design for maximum output power. A relationship for the maximum oscillator output power versus loop loss is derived. It is shown that filtering is required to suppress spurious oscillations. The output power and frequency of the designed oscillator were found to agree quite closely with calculations.

The oscillator's injection-locking performance was examined. The locking bandwidth bears an inverse relationship with the length of the transmission lines in the feedback arrangement. The locking bandwidth at 15 dB gain was found to be 69 MHz - sufficient for a transponder but not for the entire 500 MHz satcom band. The locked signal's FM noise was found to be identical to that of the injection test source for the narrow modulation bandwidth required in this application. The ILO's transient response when the FET's gate was switched ON/OFF in the presence of an input signal was determined to be spurious-free.

The following are a number of recommendations for future work:

1. Verify the design procedure in a high-power oscillator design. The performance of this high-power oscillator could be compared to another designed using the FET's measured large signal S parameters.

2. Extend the design approach to include other oscillator configurations such as series feedback.

3. Modify the computer programs used in the oscillator design to include an optimization routine for maximizing the oscillator output power at the frequency of interest.

4. Determine an FET source grounding technique which would permit easy circuit assembly. The wrap-around source tabs were difficult to keep correctly positioned when both they and the FET were being soldered into the circuit.

5. Examine the effect of varying the feedback loop's transmission line impedance on the oscillator's injection locking bandwidth.

6. Examine the temperature dependence of the oscillator's output power and stability.

6. REFERENCES

1. Hammerstad, E.O. *Equations for Microstrip Circuit Design*, 5th European Microwave Conf. Digest, 1975.

2. Maeda, M., K. Kimura and H. Kodera, *Design and Performance of X-Band Oscillators with GaAs Schottky-Gate Field Effect Transistors*, IEEE Trans. on MTT, MTT-23, No. 8, August 1975, pp. 661-667.

3. Johnson, K.M., *Large Signal GaAs MESFET Oscillator Design*, IEEE Trans. on MTT, MTT-27, No. 3, March 1979, pp. 217-227.

4. Rauscher, C., *Optimum Large-Signal Design of Fixed Frequency and Varactor-Tuned GaAs FET Oscillators*, 1980 MTT-S Symposium Digest, pp. 373-375.

5. Adler, R., *A Study of Locking Phenomena in Oscillators*, Proc. IRE, Vol. 34, June 1946, pp. 351-357.

6. Kurokawa, K., *Injection Locking of Microwave Solid-State Oscillators*, Proc. IEEE, Vol. 61, No. 10, October 1973, pp. 1386-1410.

7. Vehovec, M., L. Houselander and R. Spence, *An Oscillator Design for Maximum Power*, IEEE Trans. on CT, Sept. 1968, pp. 281-283.

8. Kotzebue, K.L. and W.J. Parrish, *The Use of Large-Signal S Parameters in Microwave Oscillator Design*, Proc. 1975, Int. Symp. on Circuits and Systems.

9. Day, W.R., G.E. Kindgren and C.C. Peterson, *Microwave Solid-State Injection Locked Amplifiers*, Microwave Journal, May 1976, pp. 59-61.

10. White, T.M., and W.B. Jones, *Frequency Transients in Synchronized Oscillators*, IEEE Trans. on CT, June 1964, pp. 279-281.

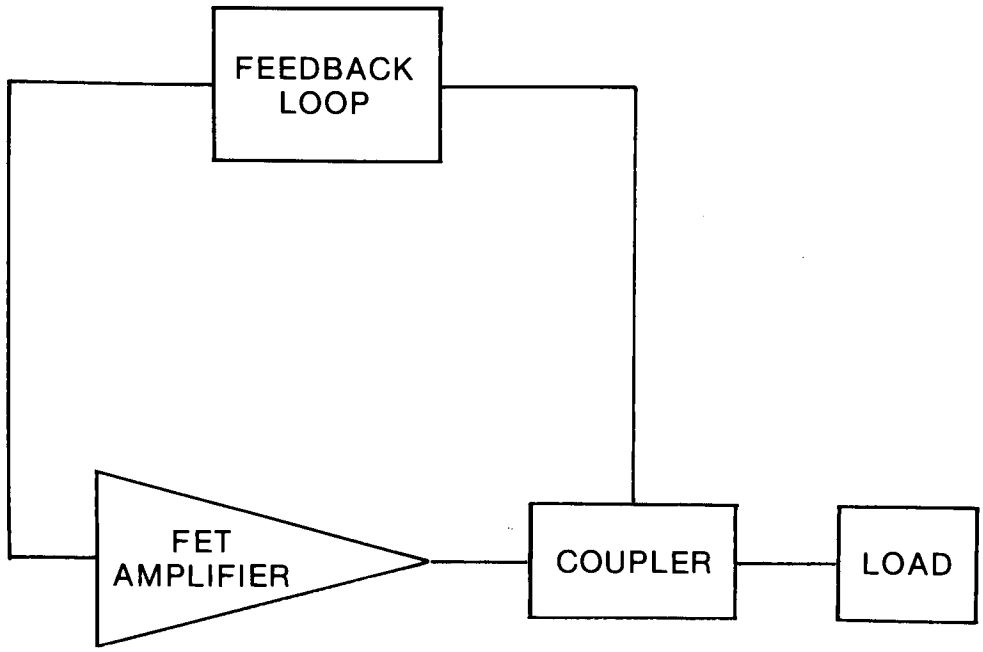

Figure 1. Shunt Oscillator Configuration

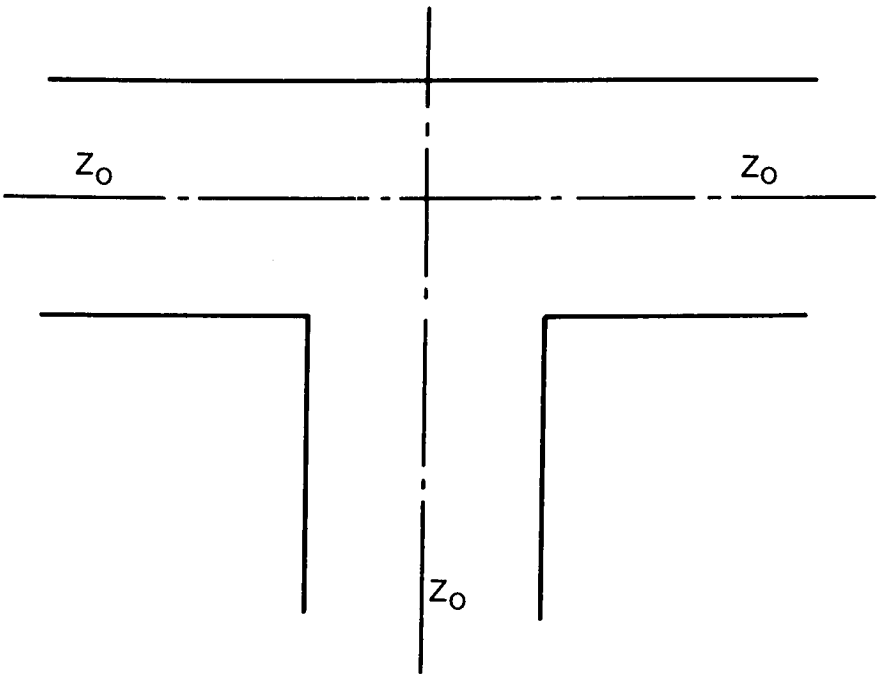

Figure 2a. Microstrip T Junction

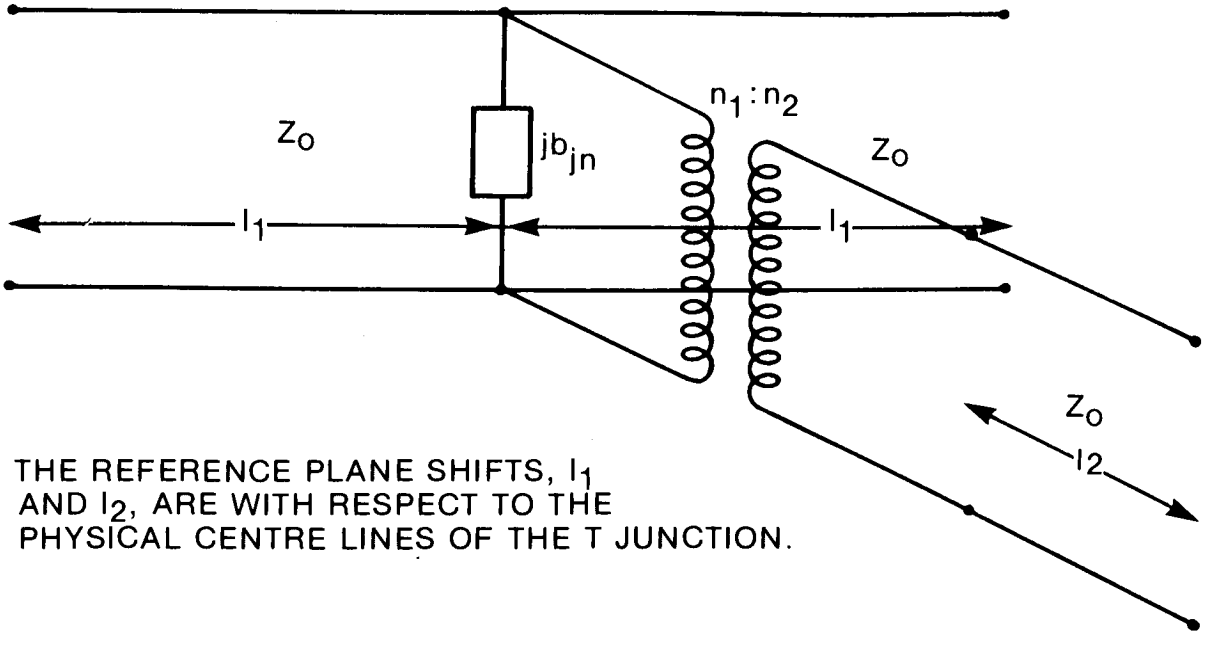

Figure 2b. Microstrip T Junction Equivalent Circuit

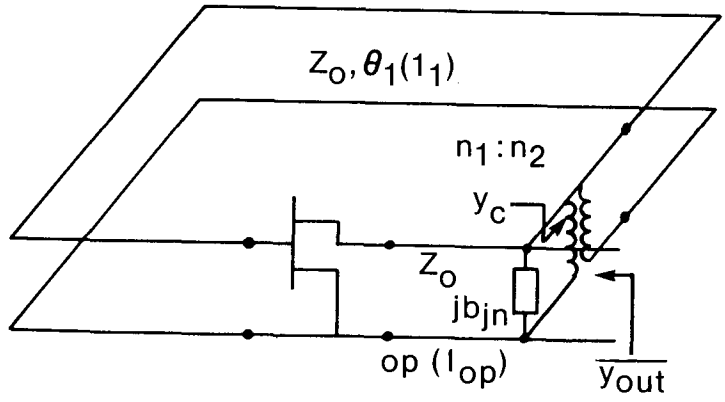

Figure 3a

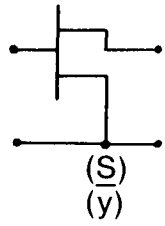

Figure 3b

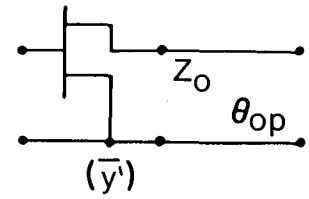

Figure 3c

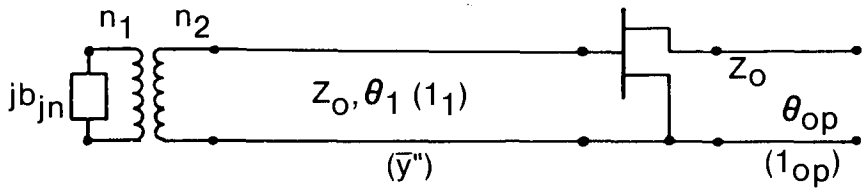

Figure 3d

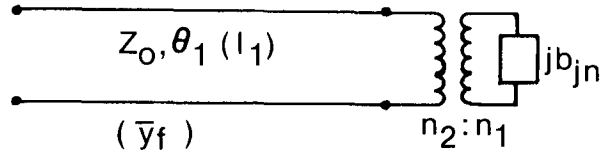

Figure 3e

Figure 3. Oscillator Sections Used in Analysis

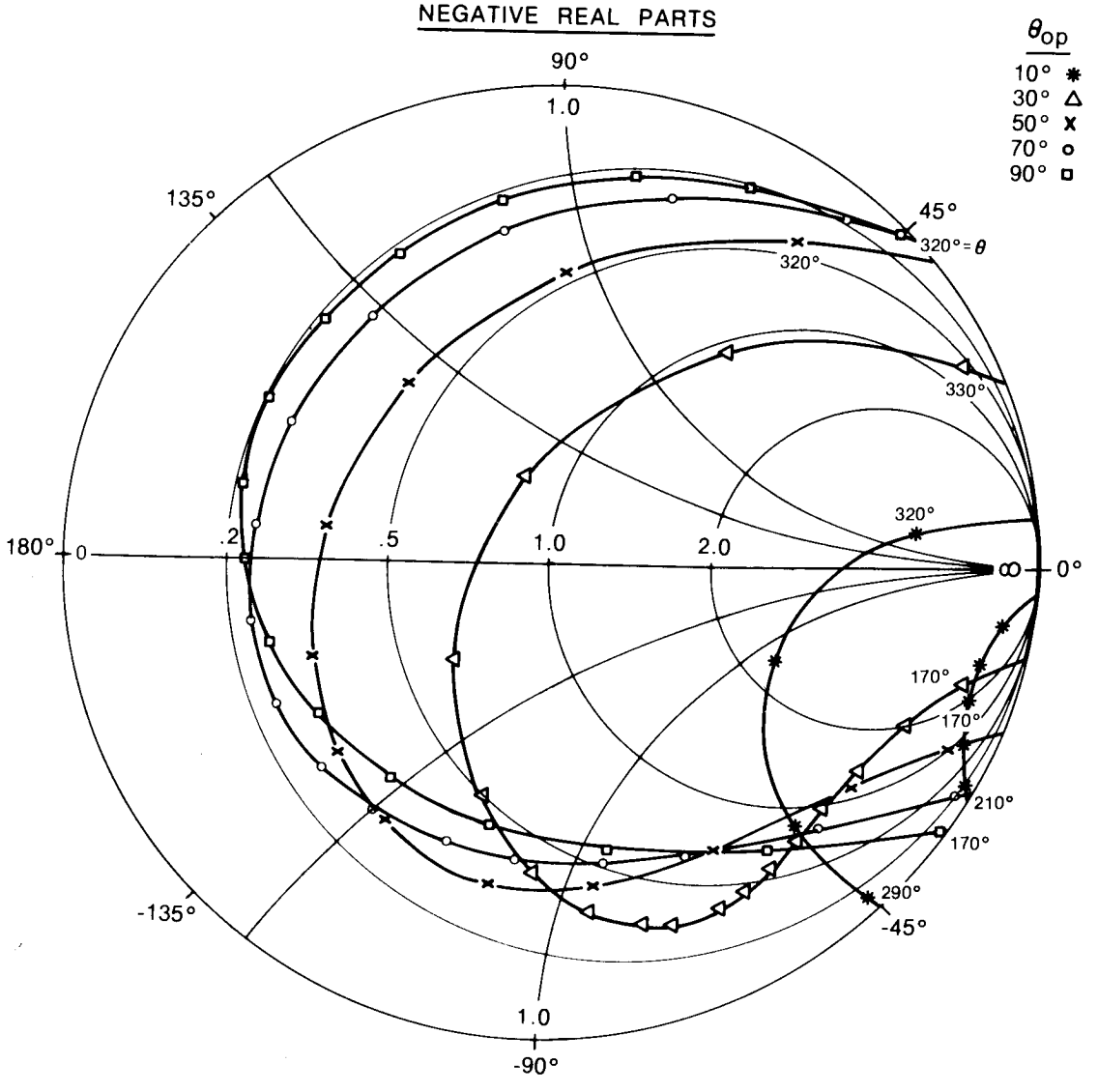

Figure 4. Small Signal Output Admittance Versus θ_1 and θ_{op}

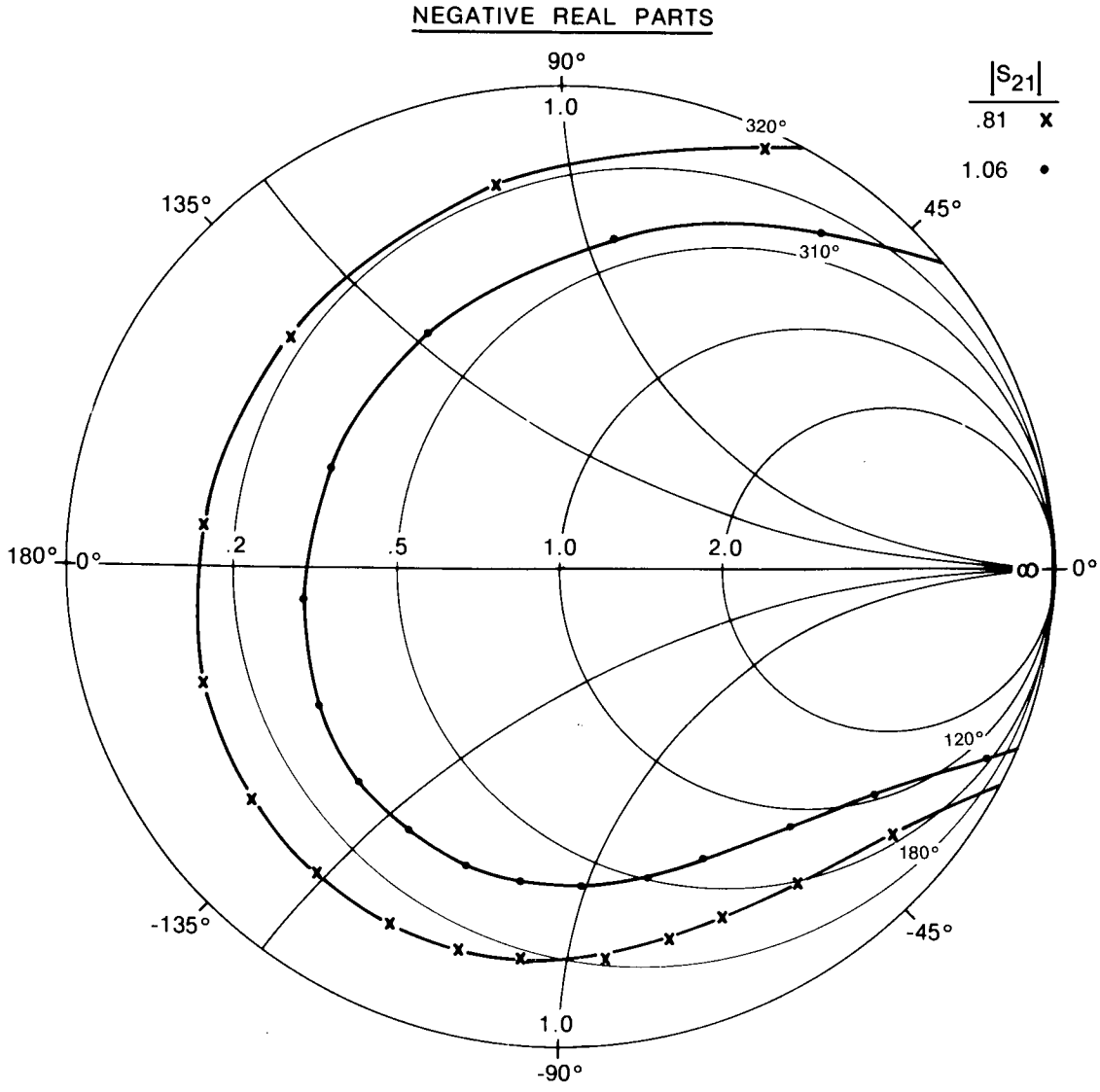

Figure 5. Output Admittance Versus S_{21}

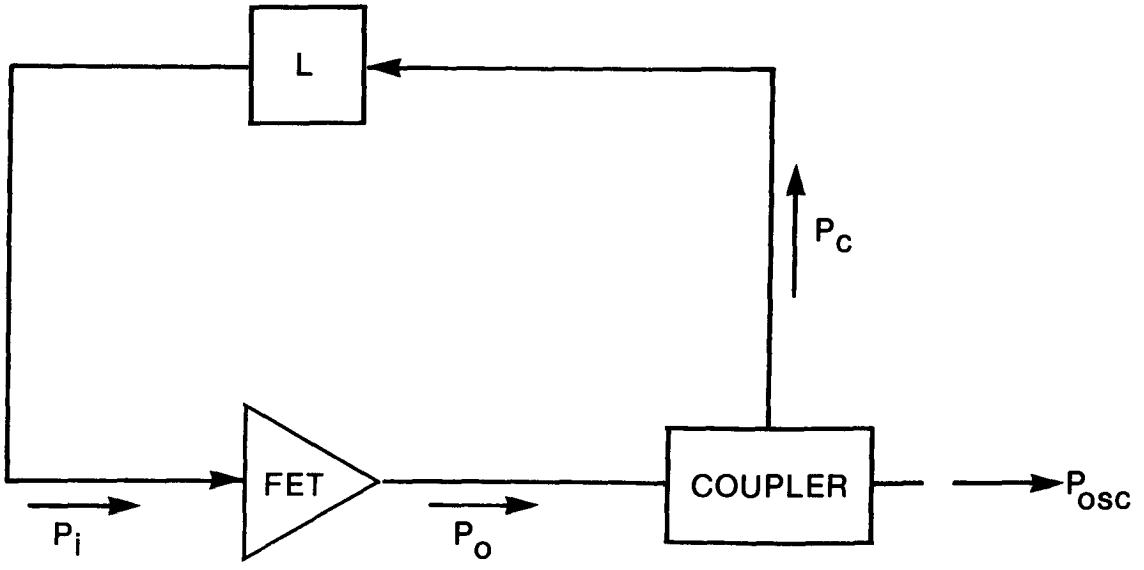

Figure 6. Oscillator Model for P_{osc} Calculations

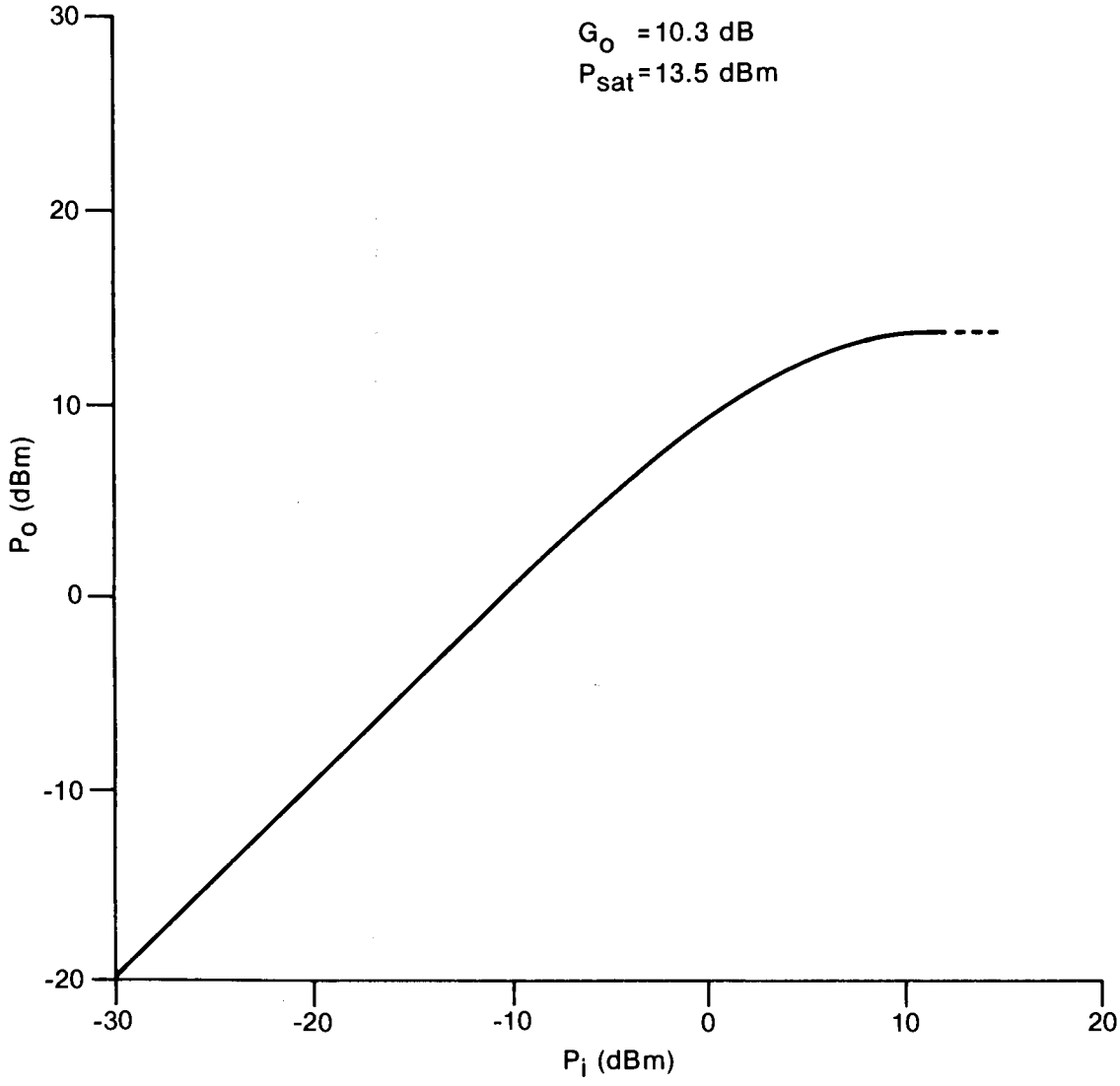

Figure 7. Amplifier P_o Versus P_i Characteristic

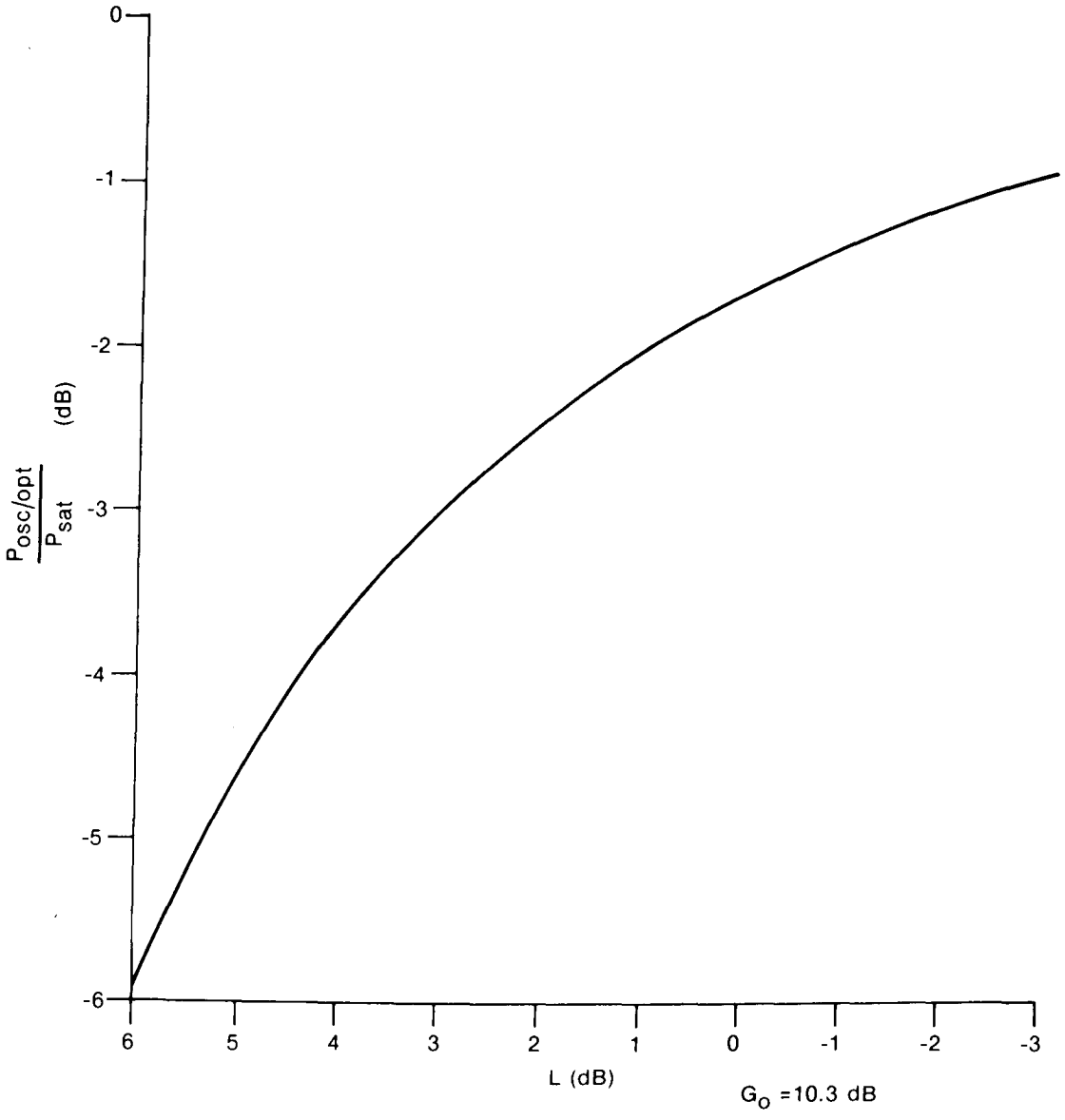

Figure 8. Maximum Oscillator Output Power Versus Feedback Loop Loss

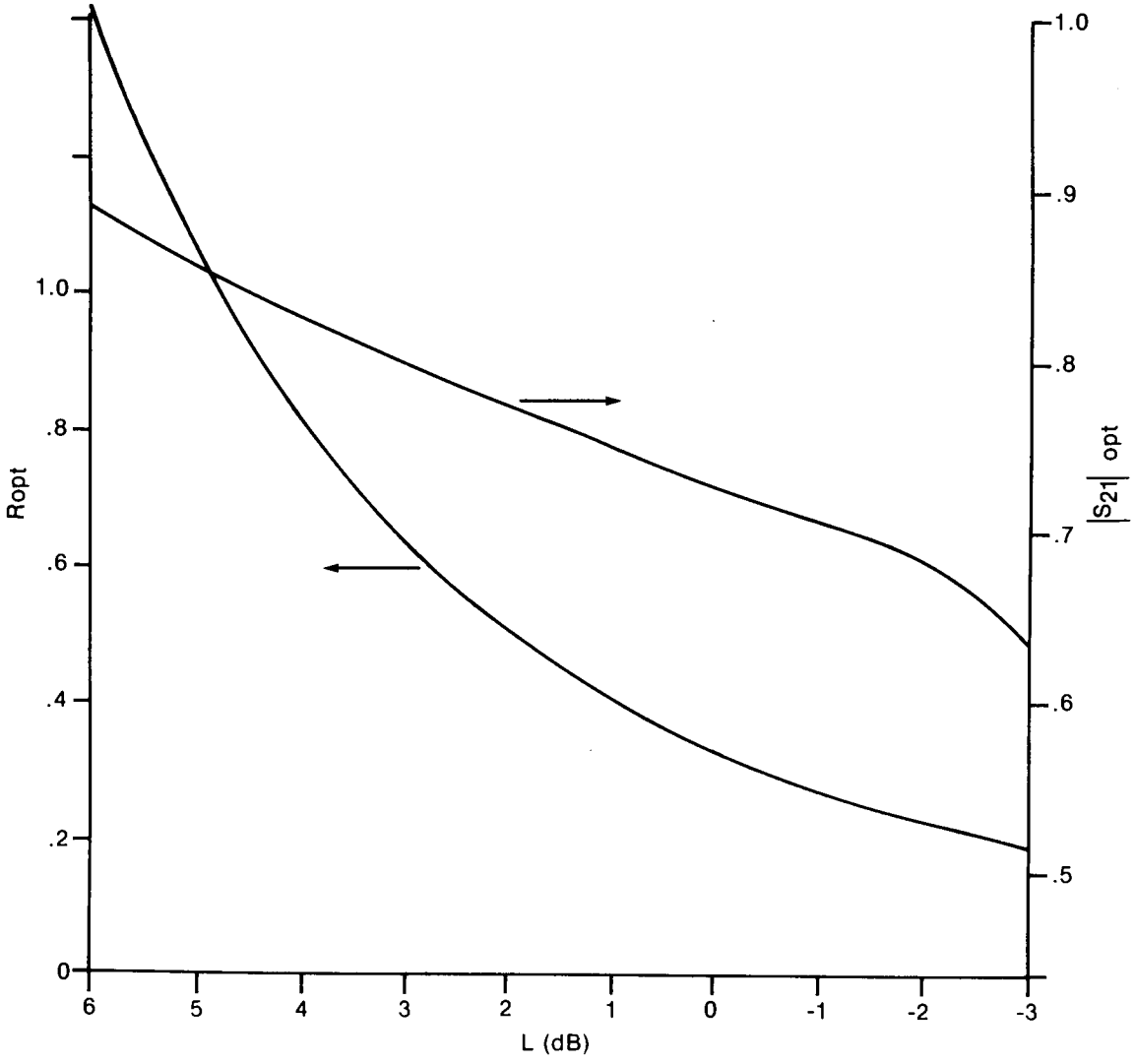

Figure 9. $|S_{21}|_{opt}$ *and* R_{opt} *Versus Feedback Loop Loss*

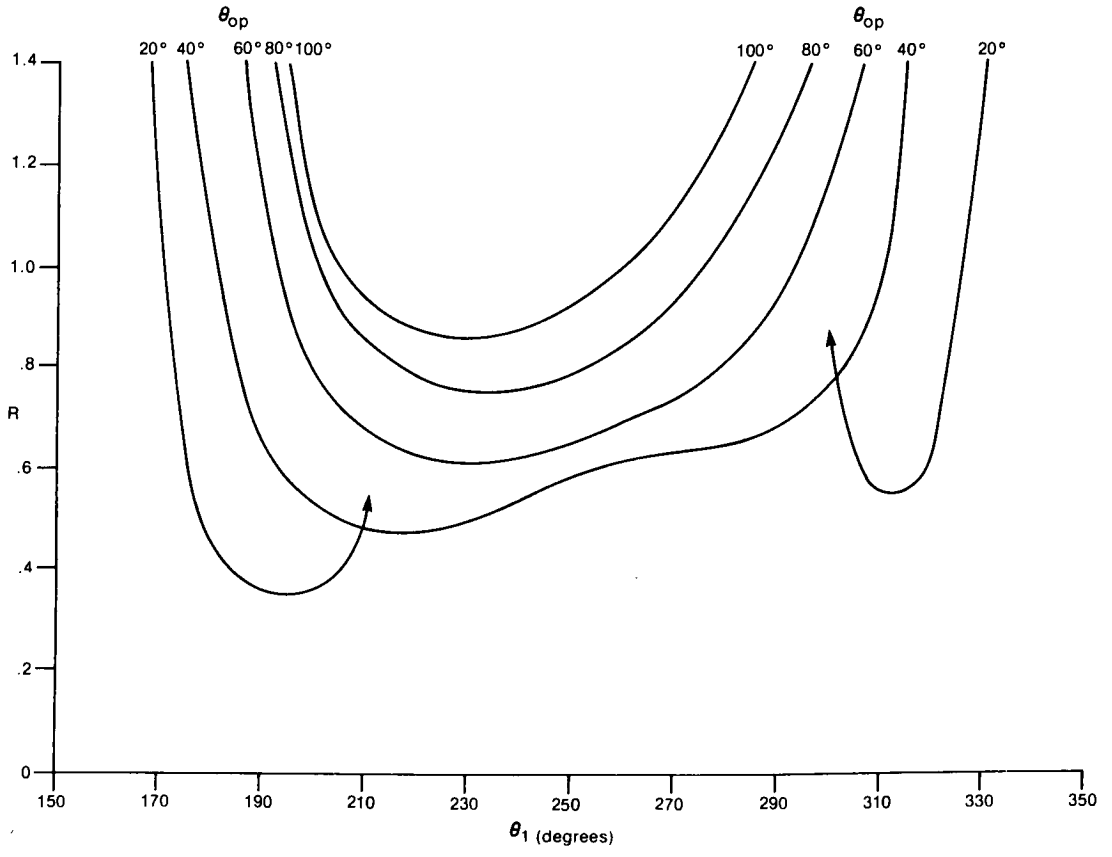

Figure 10. Coupling Ratio Versus θ_1 and θ_{op}

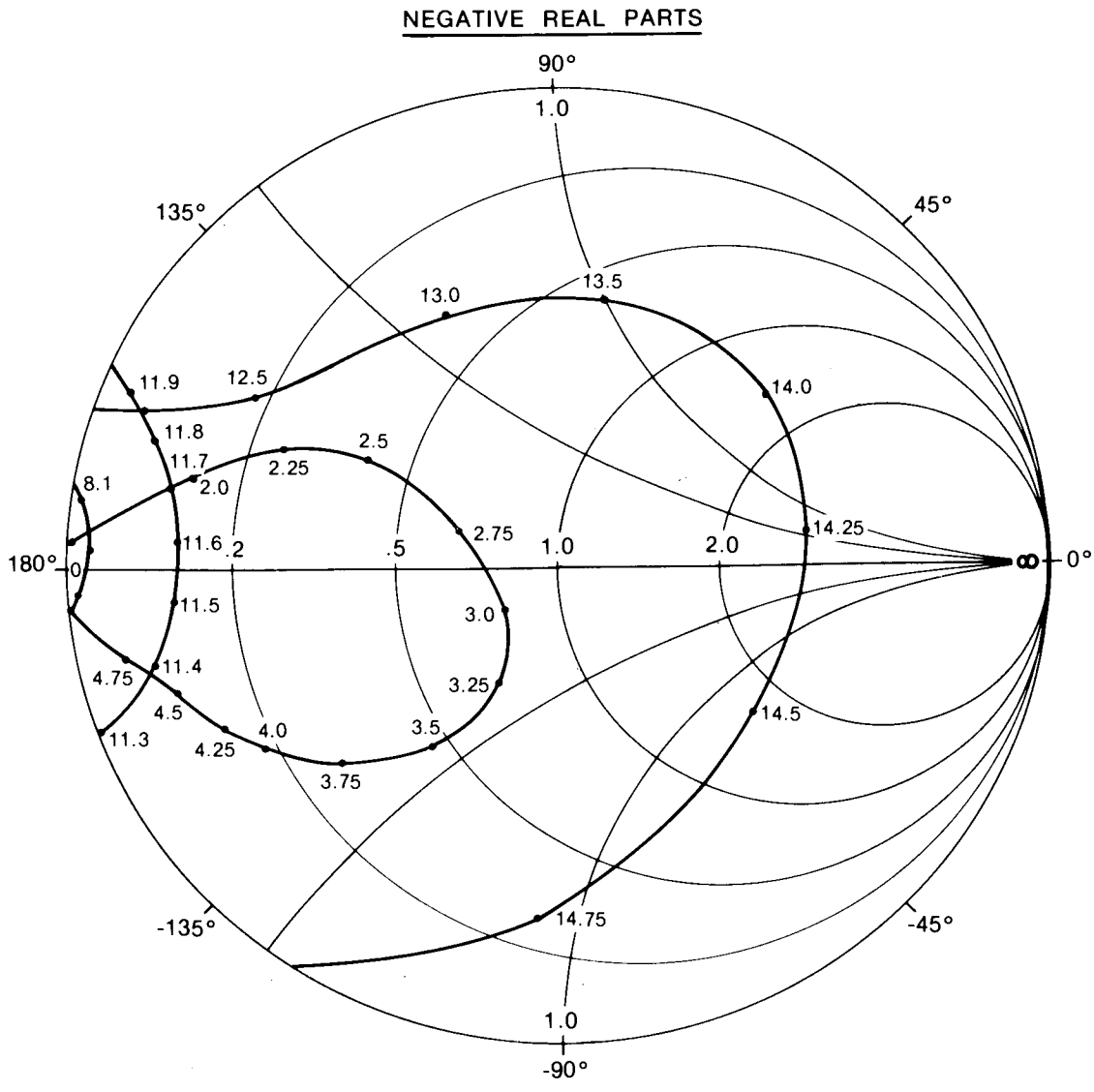

Figure 11. Output Admittance - BPF not Used

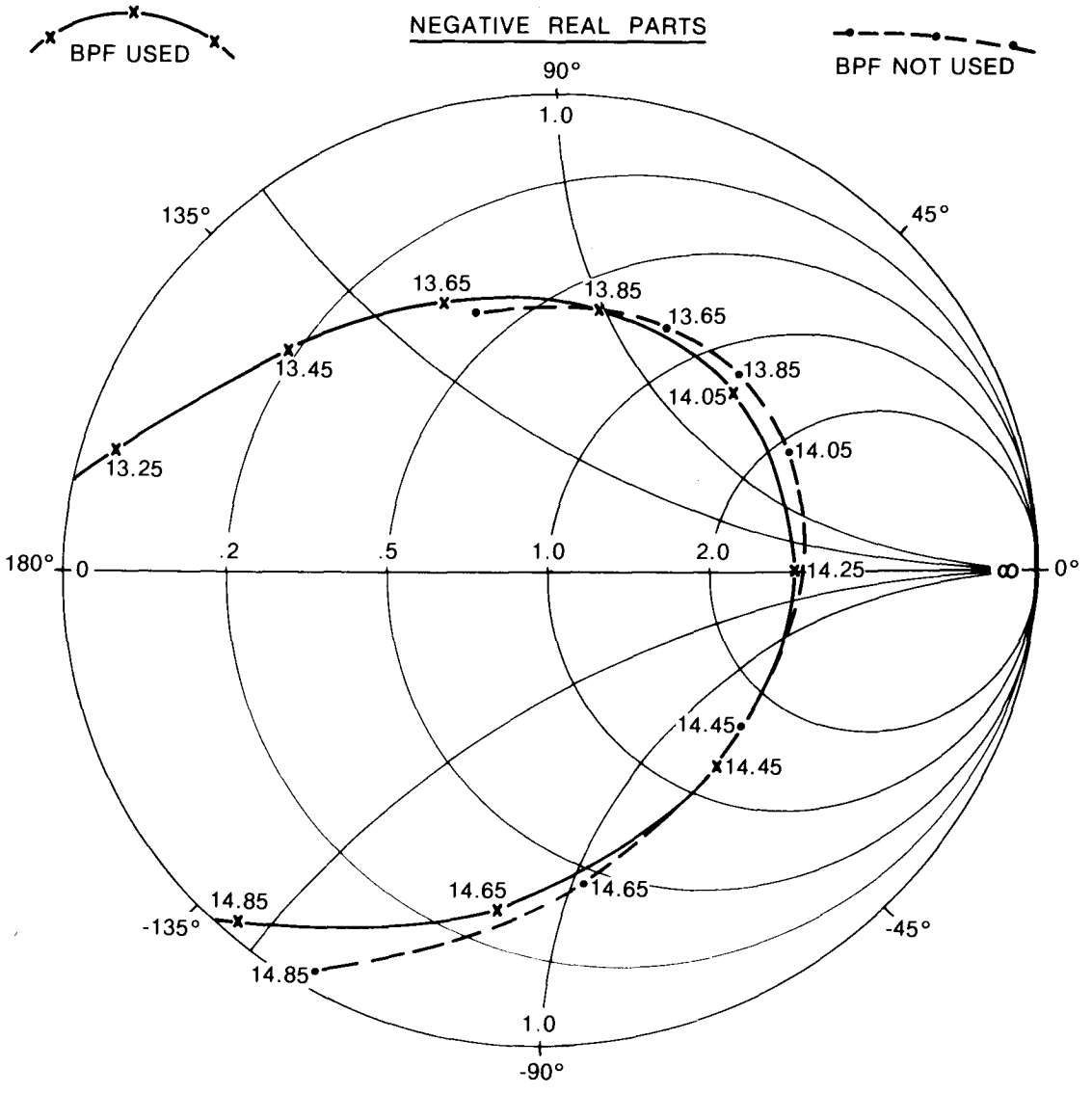

Figure 12. Small Signal Swept Frequency Output Admittance - BPF at First Position in Feedback Loop

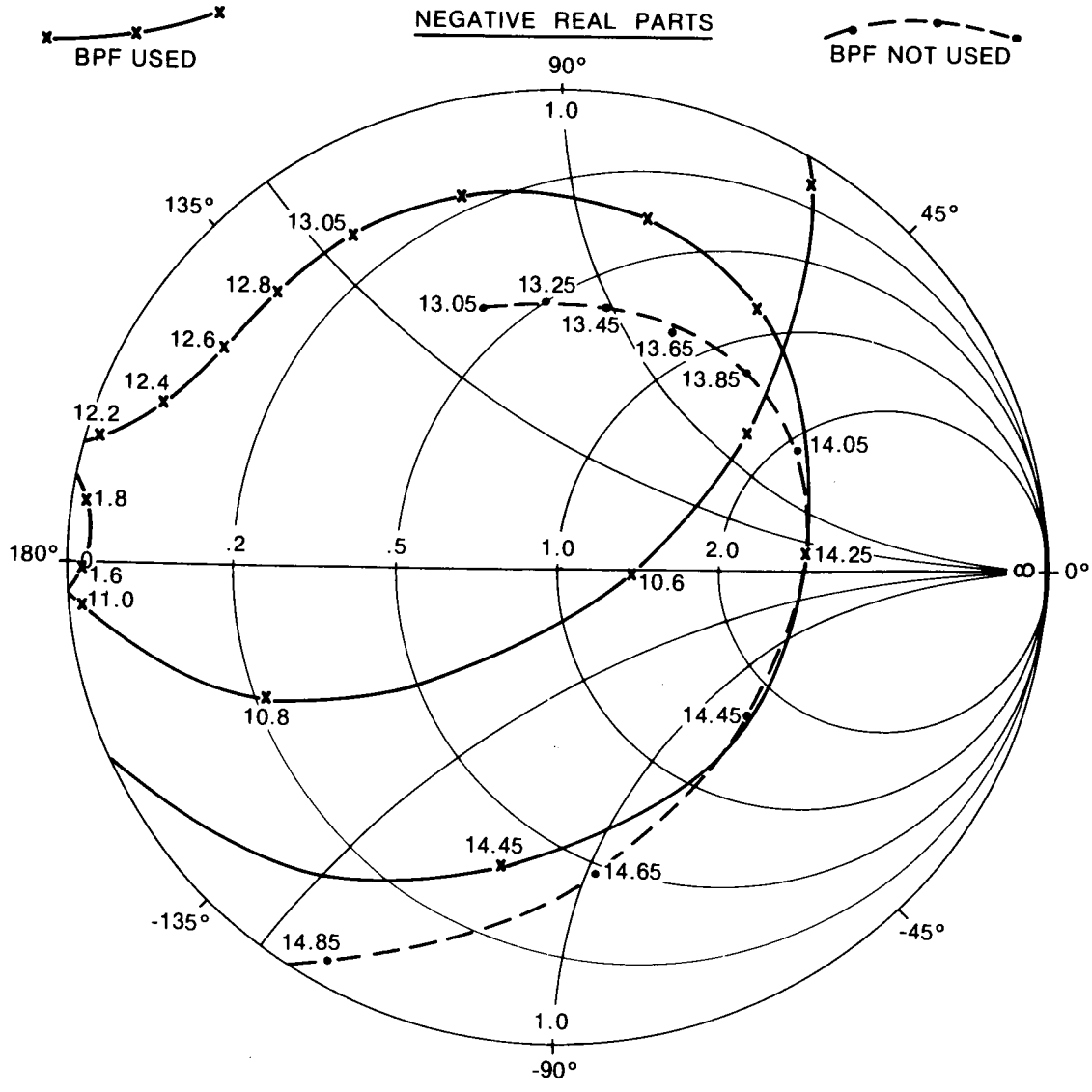

Figure 13. Small Signal Swept Frequency Output Admittance - BPF at Second Position in Feedback Loop

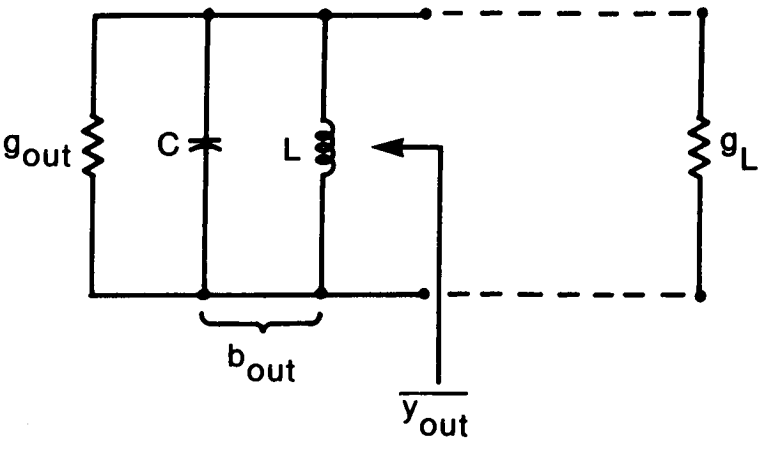

Figure 14. Output Admittance - Parallel Resonant Equivalent Circuit

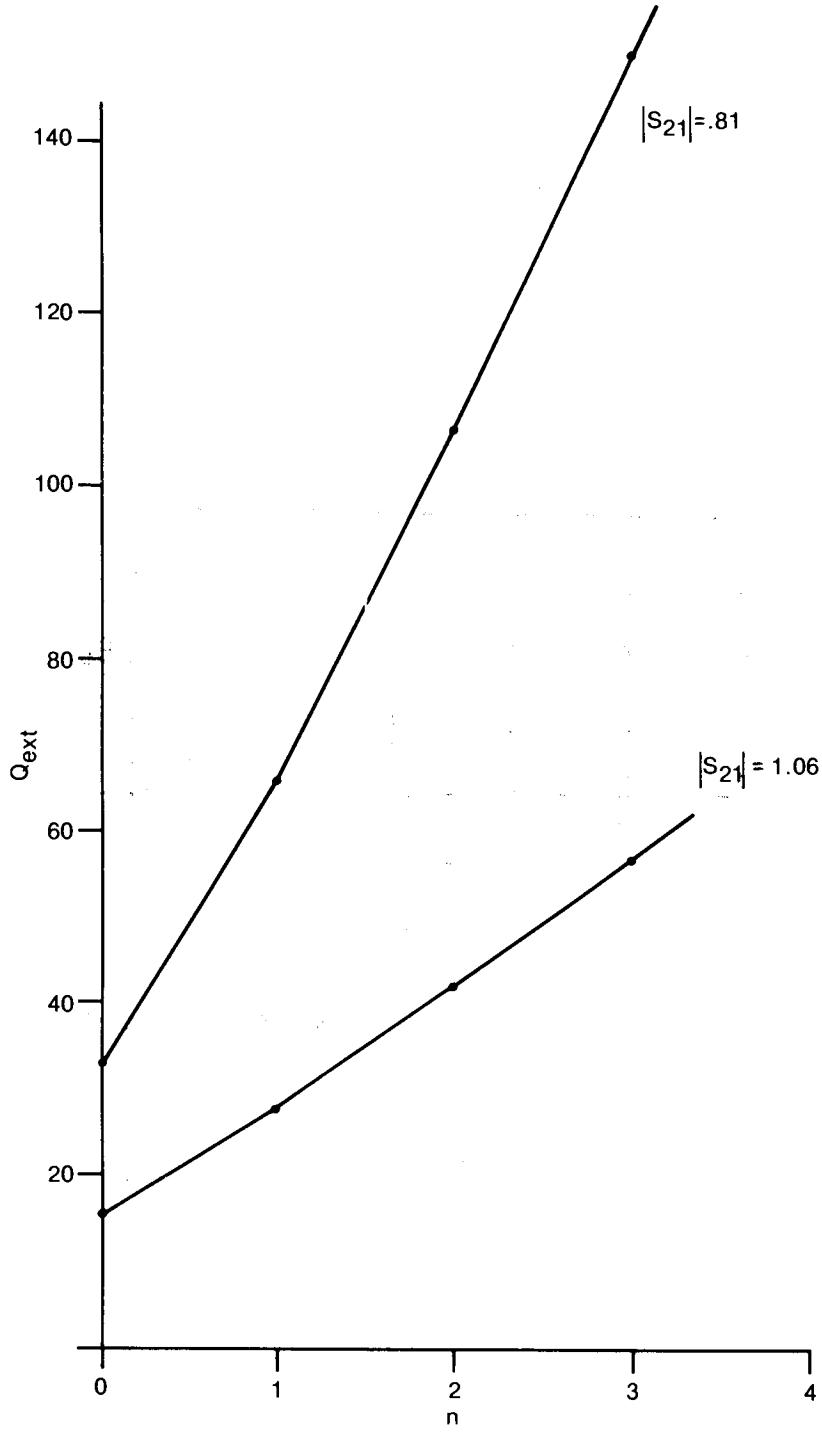

Figure 15. Q_{ext} Versus $|S_{21}|$ and Loop Length

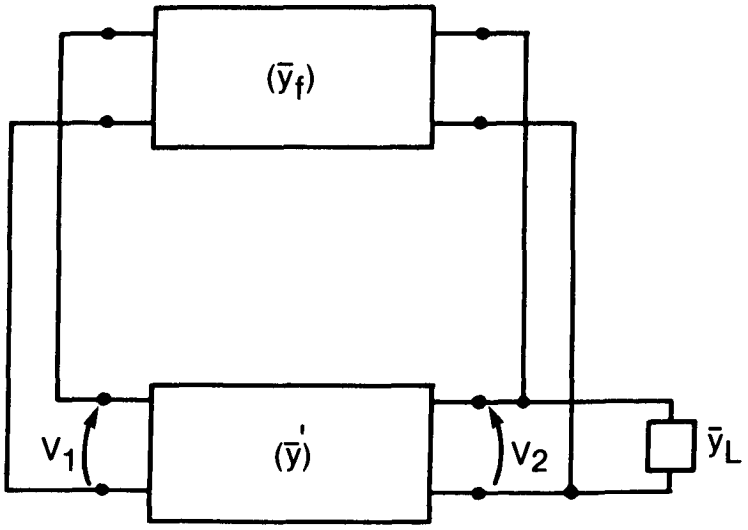

Figure 16. Equivalent Circuit for Calculation of A

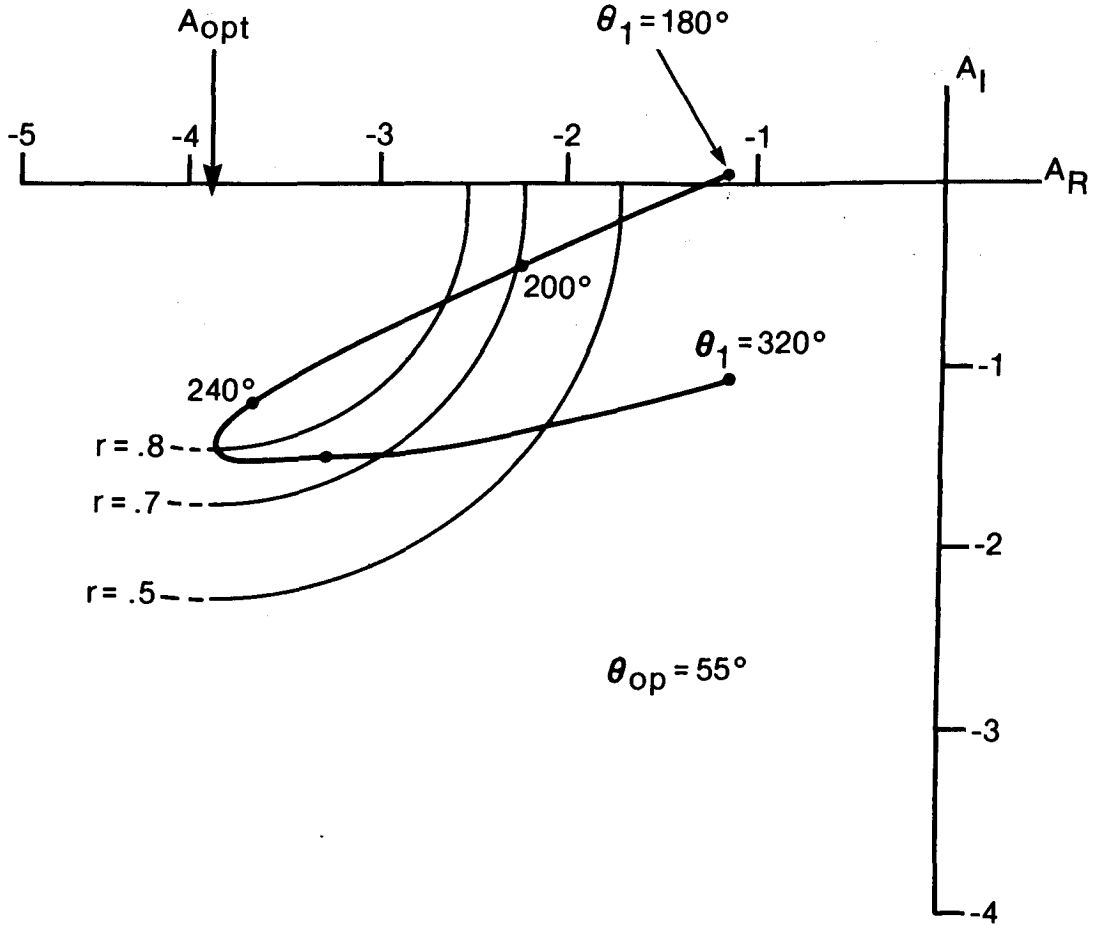

Figure 17. A Versus θ_1 for $\theta_{op} = 55°$

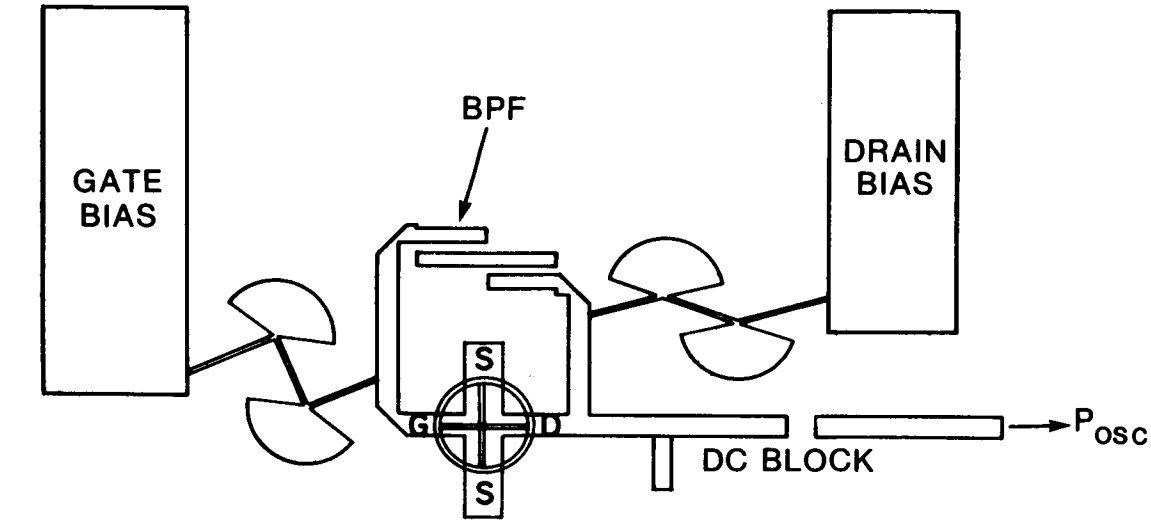

Figure 18. Oscillator Layout

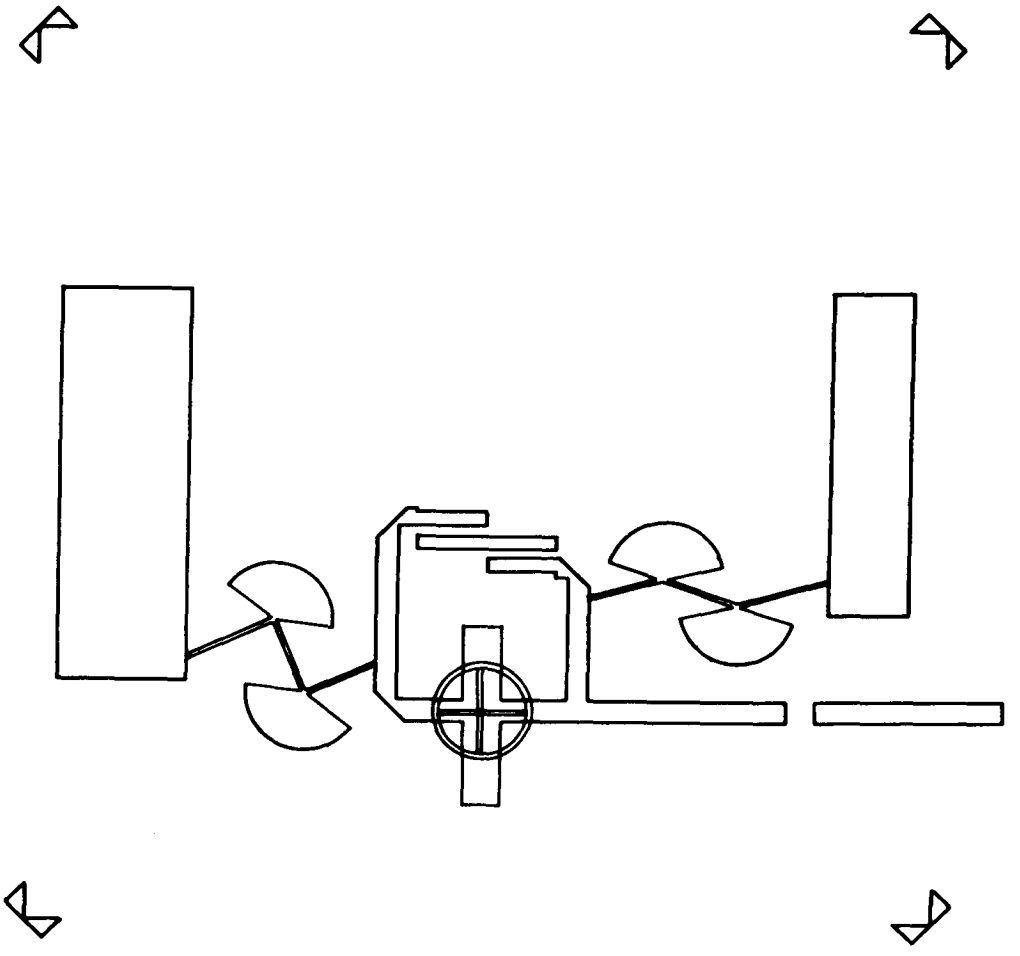

Figure 19. Oscillator Layout - Less Drain Stub

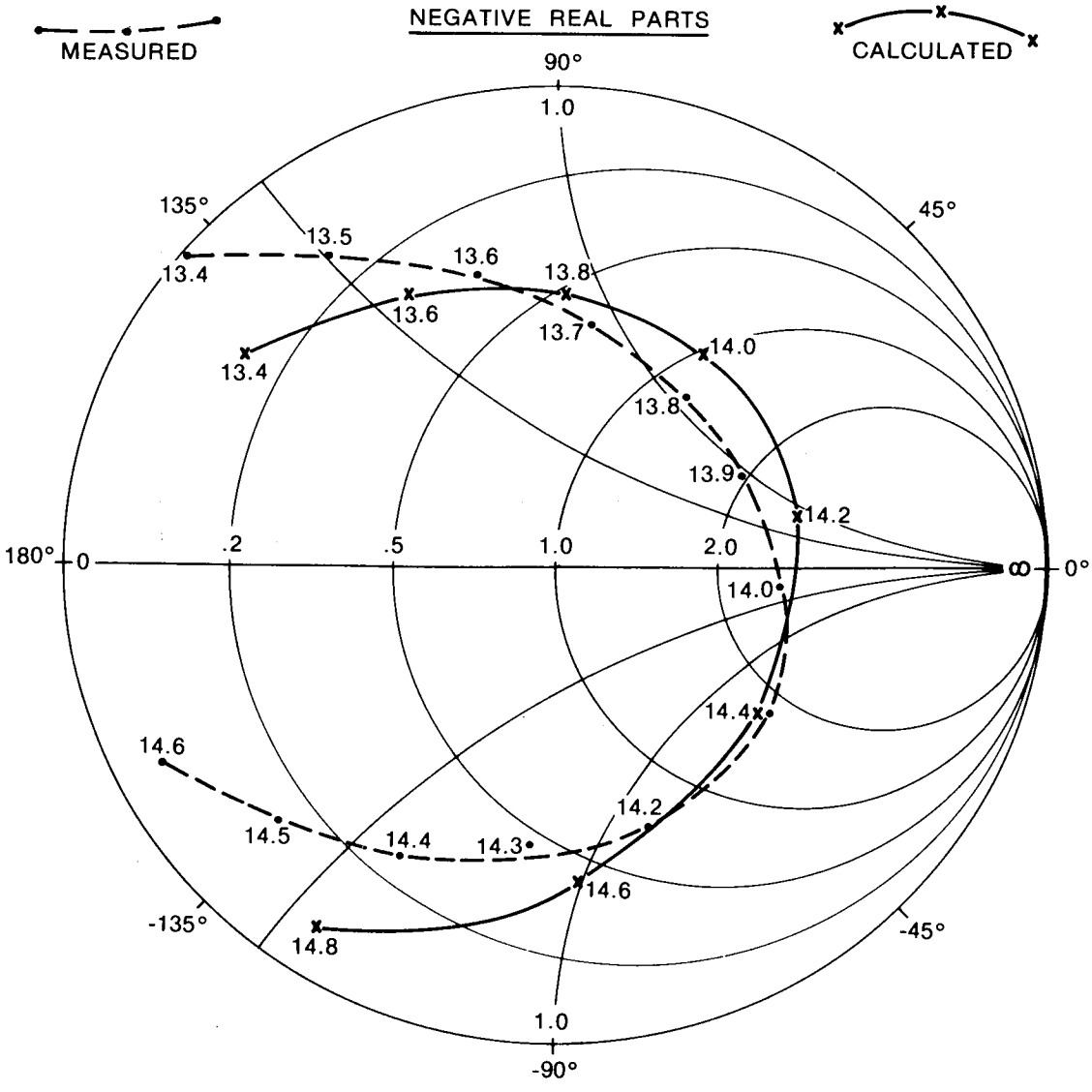

Figure 20. Measured Swept Frequency Output Admittance

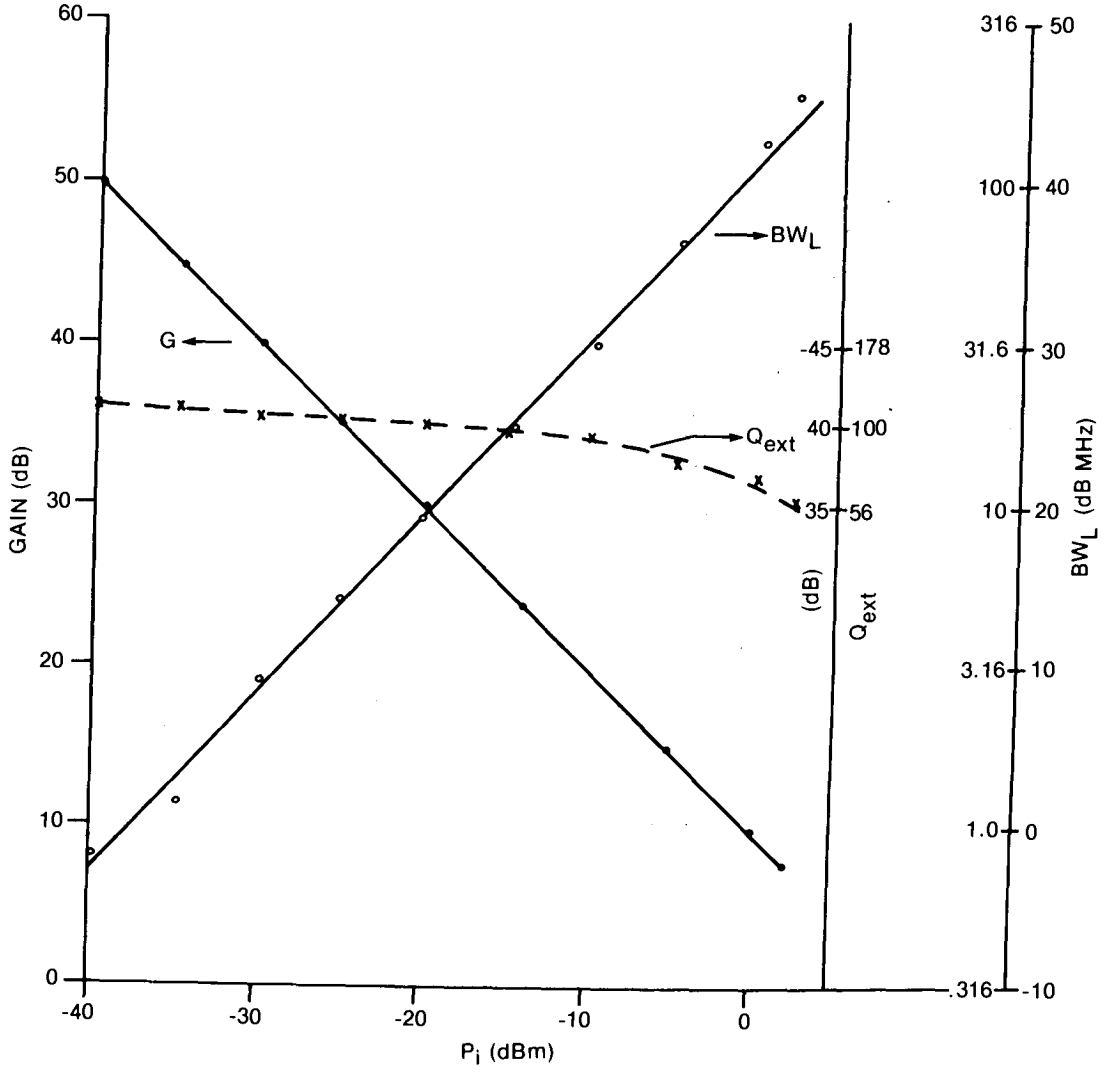

Figure 21. Injection-Locked Gain and Bandwidth Versus Injected Power

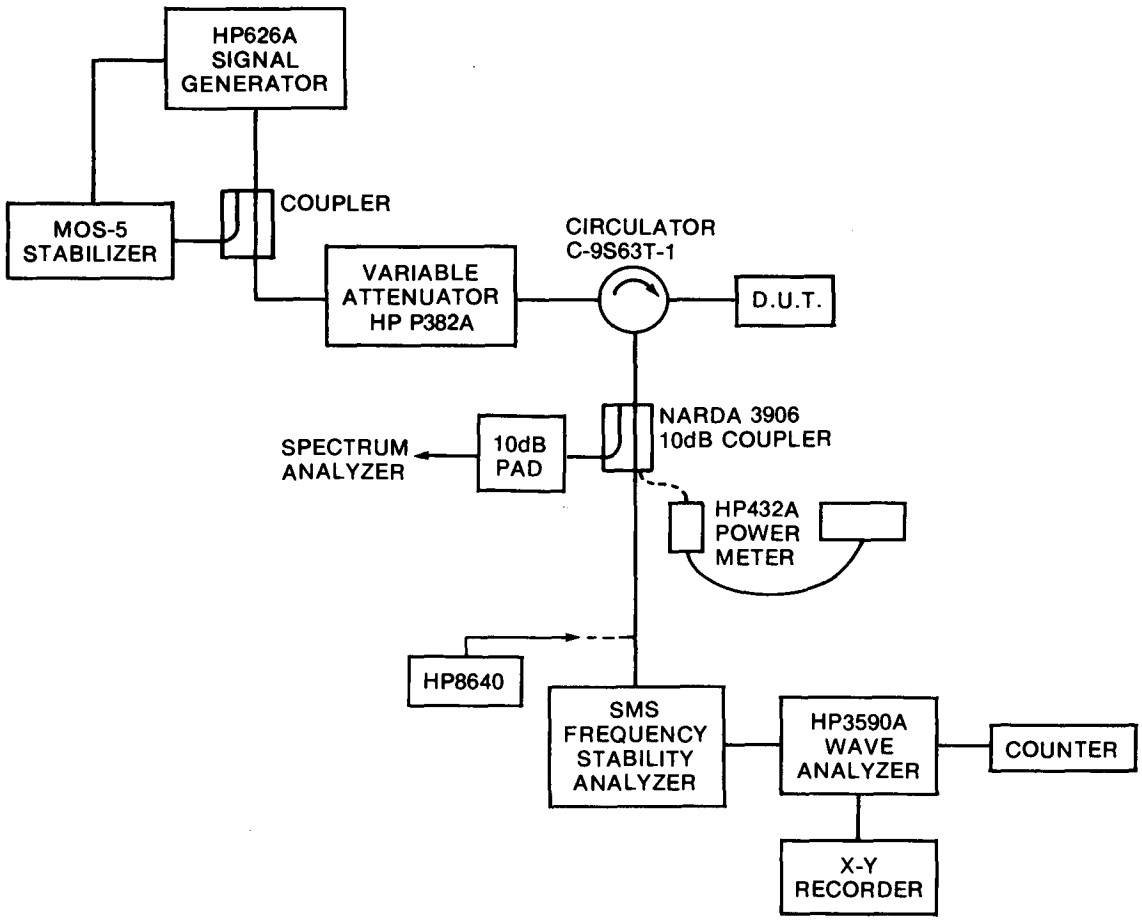

Figure 22. FM Noise Measurement Set-Up

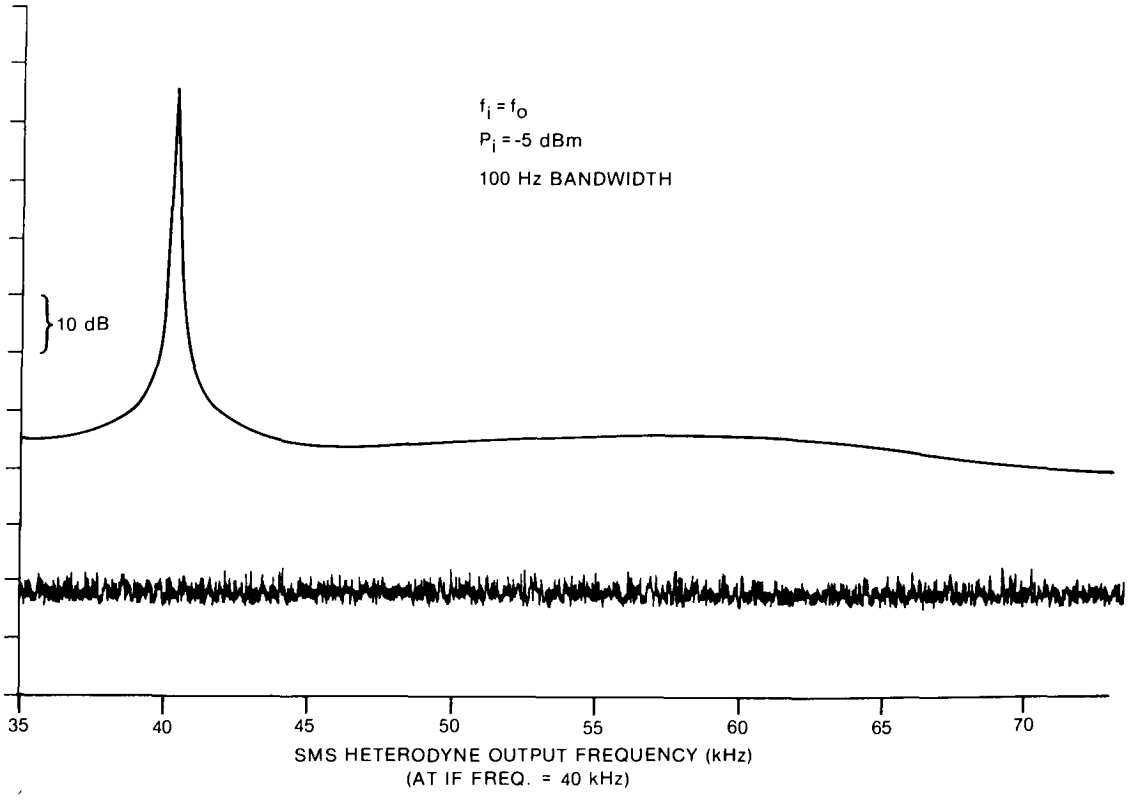

Figure 23. Injection-Locked Oscillator FM Noise Spectrum

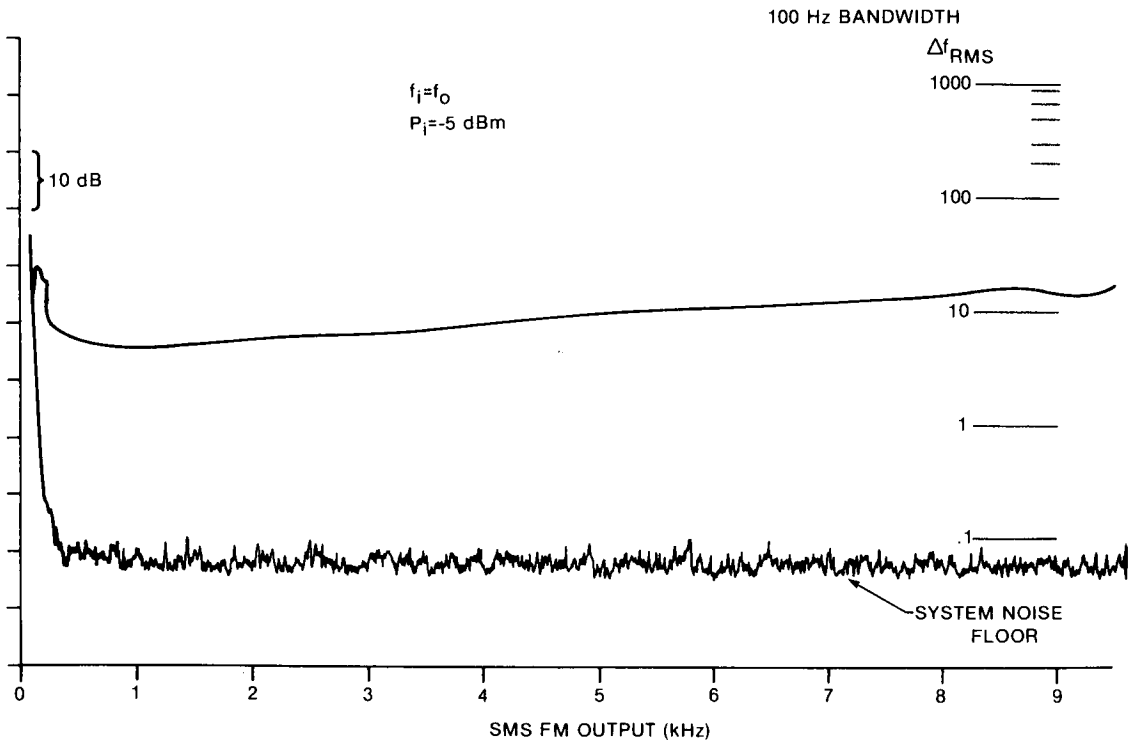

Figure 24. Injection-Locked Oscillator FM Noise Spectrum

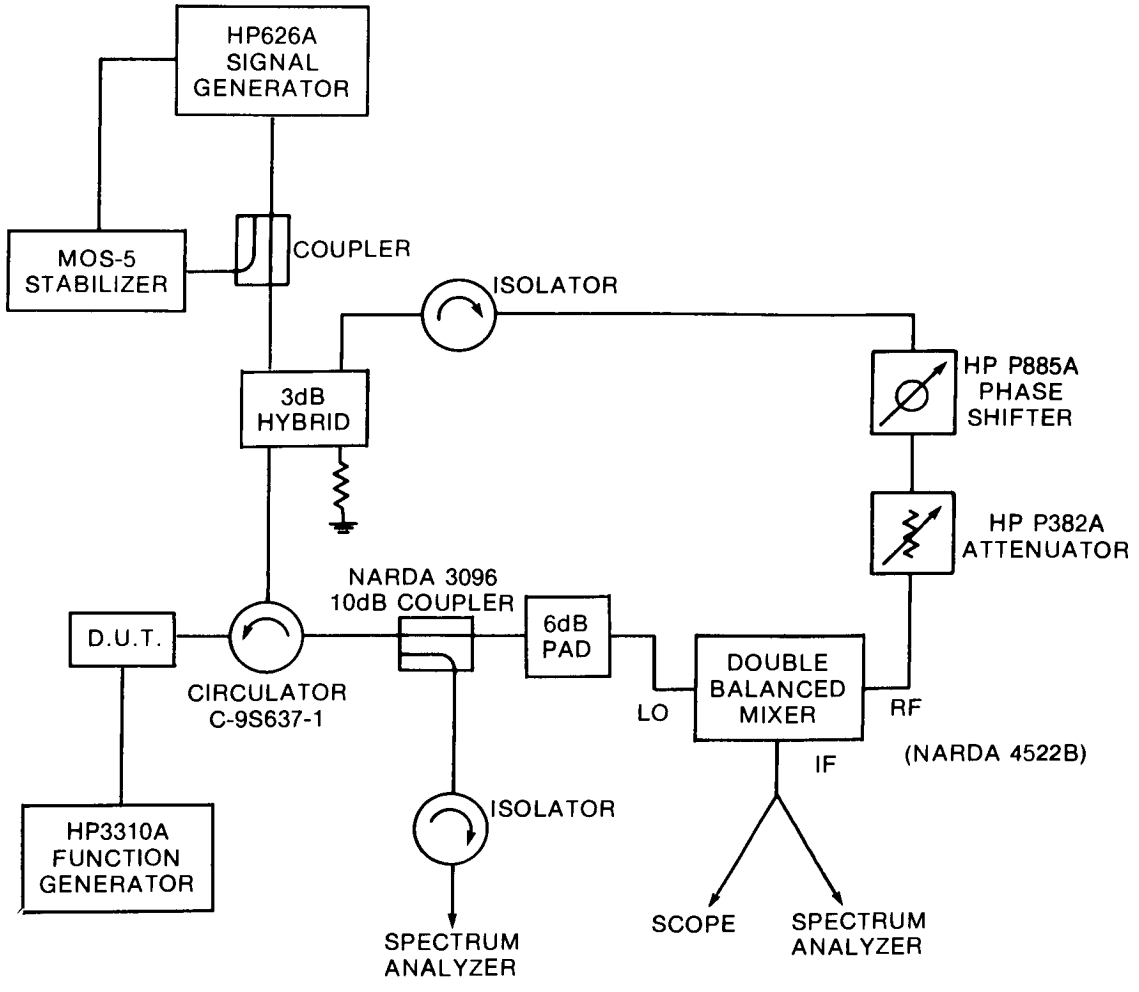

Figure 25. Transient Measurement Set-Up

CRC DOCUMENT CONTROL DATA

1. **ORIGINATOR:** Department of Communications / Communications Research Centre

2. **DOCUMENT NO:** CRC Report No. 1347

3. **DOCUMENT DATE:** January 1982

4. **DOCUMENT TITLE:** A Microwave FET Oscillator Design Approach and its Application in an Injection-Locked Oscillator

5. **AUTHOR(s):** P. Morrison and R. Douville

6. **KEYWORDS:** (1) Oscillator
(2) Microwave
(3) FET

7. **SUBJECT CATEGORY (FIELD & GROUP: COSATI)**

09 Electronics and Electrical Engineering

09 03 Electronic and Electrical Engineering

8. **ABSTRACT:** A low power 14 GHz MIC GaAs FET oscillator has been designed. The analytical model of the oscillator and design approach used are discussed in detail.

A shunt feedback oscillator configuration was employed. Approximations were made to account for FET large signal effects in the design for maximum oscillator output power. An expression relating oscillator output power to feedback loop loss is presented. The requirement for filtering in the feedback loop is discussed.

Experimental results are compared with theory and found to be in good agreement. Output power was 10 dBm at 14.0 GHz. The injection-locked characteristics of the oscillator were experimentally investigated. It was found that for a 15 dB injection gain, the locking bandwidth was 69 MHz. The FM noise properties and transient performance of the injection-locked oscillator are presented.

9. **CITATION:**

Government of Canada Gouvernement du Canada